NASA TECHNICAL NOTE

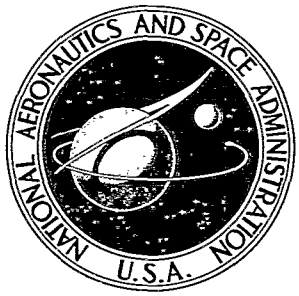

NASA TN D-5201

AERODYNAMIC INVESTIGATION OF SHARP CONE-CYLINDER SPIKES ON 120° BLUNTED CONES AT MACH NUMBERS OF 3.00, 4.50, AND 6.00

by Robert J. McGhee and W. Frank Staylor

Langley Research Center
Langley Station, Hampton, Va.

NATIONAL AERONAUTICS AND SPACE ADMINISTRATION • WASHINGTON, D. C. • JUNE 1969

AERODYNAMIC INVESTIGATION OF SHARP CONE-CYLINDER SPIKES ON 120° BLUNTED CONES AT MACH NUMBERS OF 3.00, 4.50, AND 6.00

By Robert J. McGhee and W. Frank Staylor

Langley Research Center
Langley Station, Hampton, Va.

NATIONAL AERONAUTICS AND SPACE ADMINISTRATION

For sale by the Clearinghouse for Federal Scientific and Technical Information
Springfield, Virginia 22151 – CFSTI price $3.00

AERODYNAMIC INVESTIGATION OF SHARP CONE-CYLINDER SPIKES ON 120° BLUNTED CONES AT MACH NUMBERS OF 3.00, 4.50, AND 6.00

By Robert J. McGhee and W. Frank Staylor
Langley Research Center

SUMMARY

Some effects of sharp cone-cylinder spikes located at the apex of two 120° spherically blunted cones have been investigated at free-stream Mach numbers of 3.00, 4.50, and 6.00 at angles of attack of 0°, 2°, and 5°. Spikes of various lengths, diameters, and tip angles were tested, and surface-pressure distributions and schlieren photographs were obtained for the models. The free-stream Reynolds numbers were 6.89, 2.95, and 3.64×10^6 per meter at free-stream Mach numbers of 3.00, 4.50, and 6.00, respectively.

Several distinct types of flow which occurred on the spikes were found to be a function of the parameter l/δ, the ratio of the spike-cylinder length to the bow-shock standoff distance at the stagnation point. For spike lengths of $l/\delta < 0.8$, subsonic steady flow existed over the entire model with a small region of separated flow near the spike. The bow shock was detached and unsteady in the vicinity of the spike for $0.8 < l/\delta < 1.0$. The bow shock attached to the spike tip at about $l/\delta = 1.1$ and remained steady until flow oscillation again occurred at $l/\delta > 2.2$. A region of relatively low-pressure separated flow occurred behind the attached bow shock and was followed by a high reattachment pressure near the intersection of the attached spike shock and detached body shock. The parameter l/δ correlates the separation and reattachment pressures for all spike configurations tested. The effects of spike diameter and spike-tip angle were generally small compared to the effects of spike length for the present tests.

Pressure distributions on the basic bodies (no spikes) were in good agreement with theoretical calculations, particularly on the spherical nose caps. For spike lengths of $l/\delta < 2.0$, the pressure drag was within 1 percent of the basic-body value.

INTRODUCTION

An instrumented probe extended into the region of the bow shock on a blunted entry vehicle may be used to study a number of gas-dynamics phenomena such as shock radiation and flow equilibrium. Current studies indicate that a short probe extended just

beyond the bow shock may also be very useful on planetary-entry vehicles such as those of references 1 and 2. The probe could collect uncontaminated gas samples and other data which could be analyzed to determine the gas composition, density, pressure, and temperature profiles during entry. Previous investigations, such as references 3 to 6, have shown that fairly long protruding spikes are necessary to alter significantly the total heating or drag of a body, and, therefore, short spikes have received little prior attention.

The present investigation was initiated to study the effects that a small probe located in the vicinity of the bow shock would have upon the flow field over the body. For this investigation, the probe was simulated by a solid cylindrical spike with a sharp conical tip. Spikes of various lengths, diameters, and tip angles were tested at the apex of two 120° spherically blunted cones at free-stream Mach numbers of 3.00, 4.50, and 6.00. Surface-pressure distributions and schlieren photographs were obtained for the models at angles of attack of 0°, 2°, and 5°.

SYMBOLS

C_D	drag coefficient from integrated pressures at $\alpha = 0^{\circ}$
d	spike-cylinder diameter
D_n	cone-nose diameter
D_b	cone-base diameter
l	spike-cylinder length (see table I)
L	spike total length (see table I)
M	free-stream Mach number
p	local cone-surface static pressure
$p_{t,2}$	stagnation pressure behind normal shock
Δp	local cone-surface static-pressure difference, $(p)_{\text{spike on}} - (p)_{\text{spike off}}$
r	local radius measured from cone center line

x	axial distance from cone stagnation point
α	angle of attack
δ	bow-shock standoff distance of basic body (no spike) at stagnation point at $\alpha = 0^{\circ}$
θ	spike-tip half-angle

APPARATUS AND TESTS

Models

The two 120° cone models employed in this investigation had a spherical nose bluntness D_n/D_b of 0.50 and 0.25 as shown in figure 1. The cone models had sharp shoulders and the base diameter D_b was 11.43 cm. Seven static-pressure orifices (0.15 cm in diameter) drilled perpendicular to the local-surface slope were located on the upper surface. Provision was made at the model apex for installation of a number of interchangeable spikes which were sharp cone-cylinders and whose dimensions are given in table I.

Apparatus

The tests were conducted in the 2-foot hypersonic facility at the Langley Research Center, described in reference 7. This wind tunnel is an ejector type which provides continuous flow at high Mach numbers and low densities. Simultaneous measurements of the orifice pressures were obtained from absolute pressure transducers. The data were obtained by a high-speed data acquisition system and were recorded on magnetic tape.

Tests and Accuracy

Pressure and schlieren data were obtained at free-stream Mach numbers of 3.00, 4.50, and 6.00 at angles of attack of 0°, 2°, and 5°, and schlieren photographs were also obtained for the intermediate Mach numbers of 3.50, 4.00, 5.00, and 5.50 at $\alpha = 0^{\circ}$. Since the pressure orifices were located only on the upper surface of the model, pressure data were also obtained at $\alpha = -2^{\circ}$ and -5° and are plotted at negative values of r/D_b at $\alpha = 2^{\circ}$ and 5°, respectively, in subsequent figures. The surface of the model was smooth; that is, no boundary-layer transition strips were employed, and it is believed that laminar flow existed over the entire model surface. Nominal test conditions are shown in the following table:

M	Stagnation temperature, ^{o}K	Stagnation pressure, kN/m^2	Static pressure, kN/m^2	Reynolds number per m
3.00	311	101	2.34	6.89×10^6
4.50	422	146	.58	2.95
6.00	422	319	.21	3.64

The maximum Mach number variation in the region of the test model was less than ± 0.04, and the angles of attack were believed to be accurate to $\pm 0.2^{o}$. Accuracy of the pressure transducers was ± 1 percent of the full-scale range of the gage. Each orifice of the two cone models was connected to two different pressure transducers whose full-scale ranges were 13.78 kN/m^2 and 34.47 kN/m^2. The transducer providing the better accuracy, which depended on the test Mach number, was used in measuring the local surface pressure.

RESULTS AND DISCUSSION

Surface-pressure data for all configurations tested are presented in figures 2 to 5 to illustrate the effects of angle of attack and Mach number. Surface-pressure ratios are presented in figures 6 and 7, and shock shape and bow-shock standoff distance are presented in figures 8 and 9, respectively, for the two basic body shapes (no spikes) to show the effects of nose bluntness and Mach number. Schlieren photographs of various spiked configurations are shown in figures 10 to 12 which illustrate the flow fields that existed during the test program. The effects of the spike configurations are presented in figures 13 to 15 as the increment in surface-pressure ratio referenced to the corresponding pressure on the zero-spike-length configuration. In figure 16, various flow-separation parameters are correlated as a function of spike length. The measured surface pressures were integrated to obtain the pressure drag coefficient at $\alpha = 0^{o}$ and are presented as functions of spike length in figure 17.

Aerodynamics of Basic Bodies (No Spikes)

Pressure distributions.- Pressure distributions obtained at angles of attack of 0^{o}, 2^{o}, and 5^{o} are presented in figure 2(a) for $D_n/D_b = 0.50$ and in figure 5(a) for $D_n/D_b = 0.25$. The pressure distributions increased on the windward side and decreased on the leeward side in approximately linear incremental changes with angle of attack. In figure 6, the experimental pressure distributions and theoretical solutions of reference 8 can be compared for the two models tested. The data are in good agreement with the calculated values on the spherical nose cap but are slightly underpredicted on the conical

surface. Increasing the nose bluntness D_n/D_b from 0.25 to 0.50 decreased the pressure on the conical surface which was not predicted by the solutions of reference 8. Figure 7 indicates that the pressure distributions for the smaller nose diameter, $D_n/D_b = 0.25$, are less dependent on Mach number than those for $D_n/D_b = 0.50$.

Bow-shock characteristics at $\alpha = 0^o$.- Bow-shock shapes measured at $\alpha = 0^o$ from schlieren photographs are presented in figure 8 and are compared with the theoretical shapes from reference 8. As was the case for pressure distributions, the experimental shock shapes are in good agreement with the theoretical shapes near the stagnation region but are underpredicted on the cone. Both of these underpredictions are probably caused by the inability of the theory to account for boundary-layer growth on the conical surface. In figure 9, the measured bow-shock standoff distances at the stagnation point are shown as a function of Mach number and are compared with the theoretical values of reference 8. The experimental and theoretical values are in good agreement for both configurations.

Aerodynamics of Spiked Configurations

Flow observations.- Typical schlieren photographs for spiked configurations are presented in figure 10 for both models at Mach numbers of 3.00, 4.50, and 6.00 at angles of attack of 0^o and 5^o. From these and other photographs taken during the test program, it was found that at $\alpha = 0^o$ four different types of flow occurred in the vicinity of the spikes. The types of flow that existed were found to be primarily a function of the parameter l/δ, the ratio of the spike-cylinder length to the bow-shock standoff distance at $\alpha = 0^o$, and each of the four types is illustrated in the schlieren photographs presented in figure 11.

For spike lengths of $l/\delta < 0.8$, the bow shock was steady and unaffected by the presence of the spike (fig. 11(a)). The bow shock was unsteady for $0.8 < l/\delta < 1.0$ and an oscillating bubble-like shock structure appeared at the tip of the spike (fig. 11(b)). For a spike length of about $l/\delta = 1.1$, the bow shock attached to the spike tip and was steady for $1.1 < l/\delta < 2.2$ (fig. 11(c)). The attached bow shock began to oscillate slightly at about $l/\delta = 2.2$ and the degree of oscillation generally increased with l/δ (fig. 11(d)). At an angle of attack, the bow shock was steady for short spike configurations, $l/\delta < 0.7$, but attached shocks were unsteady for all values of l/δ as can be seen in figure 10.

A schlieren photograph is presented in figure 12 for a long, large-diameter, spiked configuration at $\alpha = 0^o$ which has an attached, steady bow shock. Flow phenomena such as the regions of separated, attached, subsonic, and supersonic flow are illustrated in the photograph and in a sketch at the bottom of the figure. A close inspection of the attached bow shock in the vicinity of the spike tip reveals that the shock angle increases at the

shoulder of the spike. The free-stream flow passes through two oblique shock waves and is compressed to a pressure equal to that in the separated regions. This pressure permits the flow on the spike tip to remain attached even though the pressures and shock angles generated rearward of the tip are somewhat greater. For example, in figure 10(b) at $M = 4.50$ and $\alpha = 0^{\circ}$, the measured shock angle is about 70°, whereas the conical shock relations of reference 9 indicate that the shock angle at the tip should be 48°.

Effect of spike-tip angle.- Pressure data for spike-tip half-angles of 20°, 30°, and 40° are compared in figure 13 at $\alpha = 0^{\circ}$ with the spike-cylinder diameter d and total length L held constant. The types of flow that existed in the vicinity of the spikes were determined from schlieren photographs and are identified for each set of data in the figure. These limited data show that with increasing tip angle, the type of flow tended to change from detached to attached; however, it is believed that this flow change was caused by the slight increase in spike-cylinder length (see key in fig. 13) rather than by the tip-angle increase. For instance, at $M = 4.50$, the flow was detached for $\theta = 20^{\circ}$ $(l/\delta = 0.97)$ and $\theta = 30^{\circ}$ $(l/\delta = 1.05)$ but was attached for $\theta = 40^{\circ}$ $(l/\delta = 1.10)$. This flow phenomenon is consistent with the previously stated observation that spike lengths of about $l/\delta = 1.1$ are required for steady attached flows. The pressure distributions for a given type of flow are independent of tip angle, which further indicates that the tip angle in itself was not a primary spike variable for the present tests.

Effect of spike diameter.- Pressure data for various spike diameters are compared in figure 14 at $\alpha = 0^{\circ}$ for two values of total spike length, $L/D_b = 0.0833$ and 0.2222, with the tip half-angle held constant at 40°. These data show that the flow was attached on the longer spikes for both diameters tested but changed from detached to attached flow with decreasing spike diameter for the shorter spikes. Similar to the tip-angle phenomenon, it is believed that this flow change was caused by the slight increase in spike-cylinder length (see key in fig. 14) rather than by the diameter decrease. For instance, at $M = 4.50$ the flow is detached for $d/D_b = 0.0444$ $(l/\delta = 0.81)$ but is attached for $d/D_b = 0.0111$ $(l/\delta = 1.10)$ and $d/D_b = 0.0044$ $(l/\delta = 1.15)$. The pressure distributions in the vicinity of the spike were generally independent of spike diameter for a given type of flow.

Effect of spike length.- Pressure data for various spike lengths are compared in figure 15 at $\alpha = 0^{\circ}$ with the spike diameter and tip angle held constant. These data show that spike length has a more prominent effect on the pressure distributions than did the spike diameter or tip angle. With increasing spike length, the pressure decreases in the separated region and the point of reattachment moves outward. The pressure rise $\Delta p/p_{t,2}$ at flow reattachment increases with spike length; however, the magnitude of the reattachment pressure was approximately stagnation pressure $\left(p/p_{t,2} \approx 1.0\right)$ at $\alpha = 0^{\circ}$

for all spikes tested. At an angle of attack, the reattachment pressure generally exceeded stagnation pressure when the flow was attached to the spike tip. (See figs. 2 to 5.)

Correlation of spike pressure data at $\alpha = 0^{\circ}$.- The separation pressures at $r/D_b = d/2D_b$ and the maximum pressures at flow reattachment are presented in figure 16 as a function of l/δ for $\alpha = 0^{\circ}$. The data points were obtained from fairing the data of figures 13 to 15 and include the variables of model-nose diameter, Mach number, spike length, diameter, and tip angle. In general, both the separation and reattachment pressures were well correlated by the parameter l/δ and did not show obvious dependence on any other variable. These correlations tend to confirm earlier observations that the types of flow that existed in the vicinity of the spikes were a function of l/δ.

Effect of pressure drag coefficient.- Integrated-pressure drag coefficients C_D at $\alpha = 0^{\circ}$ are presented in figures 17(a) and 17(b) as a function of the spike length l/D_b for $\theta = 40^{\circ}$ and $d/D_b = 0.0111$. The drag coefficient decreased with Mach number for both basic bodies, although C_D for the small-nose-diameter model $\left(D_n/D_b = 0.25\right)$ was nearly constant. In figure 17(c) the values of $C_D/C_{D,\text{no spike}}$ at $M = 3.00$, 4.50, and 6.00 for both models are plotted as a function of the spike parameter l/δ. The data are reasonably correlated for $l/\delta < 2.0$ but show a dependence on Mach number for $l/\delta > 2.0$. For $l/\delta = 1.0$, the increase in drag was negligible, and even for $l/\delta = 2.0$ the drag coefficient was within 1 percent of the basic-body value.

CONCLUDING REMARKS

Some effects of sharp cone-cylinder spikes located at the apex of two 120° spherically blunted cones have been investigated at free-stream Mach numbers of 3.00, 4.50, and 6.00 at angles of attack of 0°, 2°, and 5°. Spikes of various lengths, diameters, and tip angles were tested, and surface-pressure distributions and schlieren photographs were obtained for the models. The free-stream Reynolds numbers were 6.89, 2.95, and 3.64×10^6 per meter at free-stream Mach numbers of 3.00, 4.50, and 6.00, respectively.

For the present tests, it was found that most of the flow phenomena produced by the spikes were a function of the parameter l/δ, the ratio of the spike-cylinder length to the bow-shock standoff distance at the stagnation point. Separation pressure, reattachment pressure, and drag-coefficient increase were correlated as a function of l/δ at an angle of attack of 0° for all the variables of the test program. The bow shock in the vicinity of the spike progressed from steady detached, unsteady detached, steady attached, to unsteady attached for increasing l/δ at $\alpha = 0^{\circ}$. At an angle of attack, it was observed that attached shocks were unsteady for all values of l/δ.

The effects of spike diameter and spike-tip angle were generally small compared to the effects of spike length. Steady attached flow was maintained on the spike tip with a drag increase of less than 1 percent.

Langley Research Center,
National Aeronautics and Space Administration,
Langley Station, Hampton, Va., April 14, 1969,
124-07-02-32-23.

REFERENCES

1. Bernot, Peter T.: Longitudinal Stability Characteristics of Several Proposed Planetary Entry Vehicles at Mach 6.73. NASA TN D-2785, 1965.

2. Campbell, James F.; and Howell, Dorothy T.: Supersonic Aerodynamics of Large-Angle Cones. NASA TN D-4719, 1968.

3. Album, Hyman H.: Spiked Blunt Bodies in Supersonic Flow. AFOSR Rep. 307, U.S. Air Force, June 1961.

4. Sims, William H.; and Hahn, Jerry S.: Aerodynamic Drag on Spiked Blunt Bodies in Low-Density Hypersonic Flow. AEDC-TDR-64-160, U.S. Air Force, Aug. 1964.

5. Bogdonoff, Seymour M.; and Vas, Irwin E.: Preliminary Investigations of Spiked Bodies at Hypersonic Speeds. J. Aero Space Sci., vol. 26, no. 2, Feb. 1959, pp. 65-74.

6. Holden, Michael S.: Experimental Studies of Separated Flows at Hypersonic Speeds. Part I: Separated Flows Over Axisymmetric Spiked Bodies. AIAA J., vol. 4, no. 4, Apr. 1966, pp. 591-599.

7. Stokes, George M.: Description of a 2-Foot Hypersonic Facility at the Langley Research Center. NASA TN D-939, 1961.

8. South, Jerry C., Jr.: Calculation of Axisymmetric Supersonic Flow Past Blunt Bodies With Sonic Corners, Including a Program Description and Listing. NASA TN D-4563, 1968.

9. Ames Research Staff: Equations, Tables, and Charts for Compressible Flow. NACA Rep. 1135, 1953. (Supersedes NACA TN 1428.)

TABLE I.- SPIKE CONFIGURATIONS TESTED

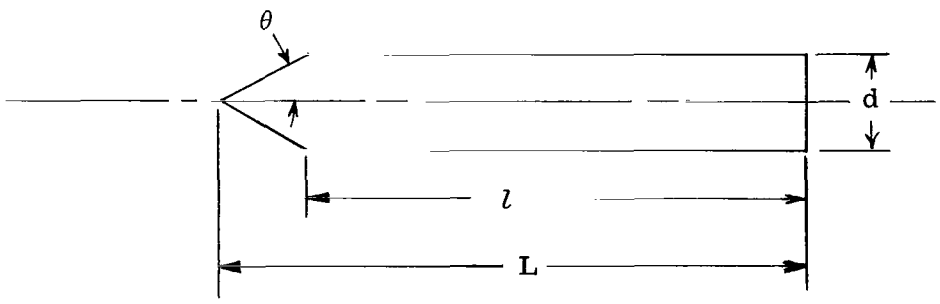

Spike configurations			
θ, deg	l/D_b	d/D_b	L/D_b
40	0.0489	0.0111	0.0555
40	.0767	.0111	.0833
40	.1045	.0111	.1111
40	.1601	.0111	.1667
40	.2156	.0111	.2222
40	.0807	.0044	.0833
40	.0568	.0444	.0833
40	.1892	.0555	.2222
30	.0737	.0111	.0833
20	.0680	.0111	.0833

Orifice location	
Orifice number	r/D_b
1	0.033
2	.065
3	.096
4	.125
5	.240
6	.360
7	.460

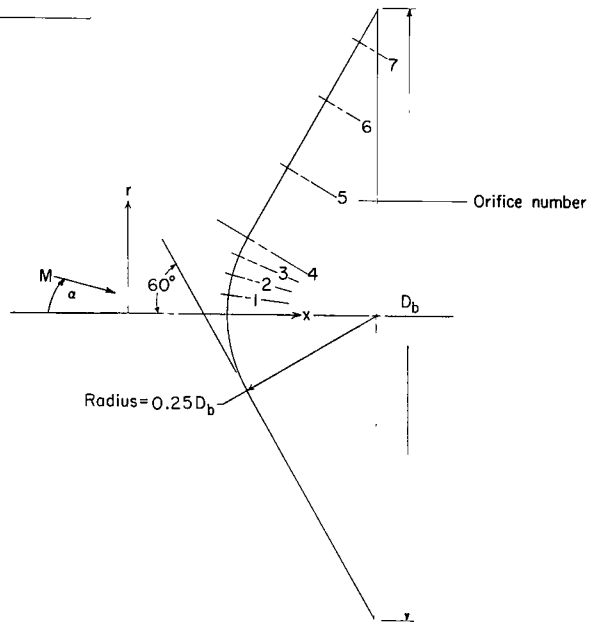

(a) $D_n/D_b = 0.50$.

Orifice location	
Orifice number	r/D_b
1	0.033
2	.062
3	.111
4	.167
5	.222
6	.333
7	.444

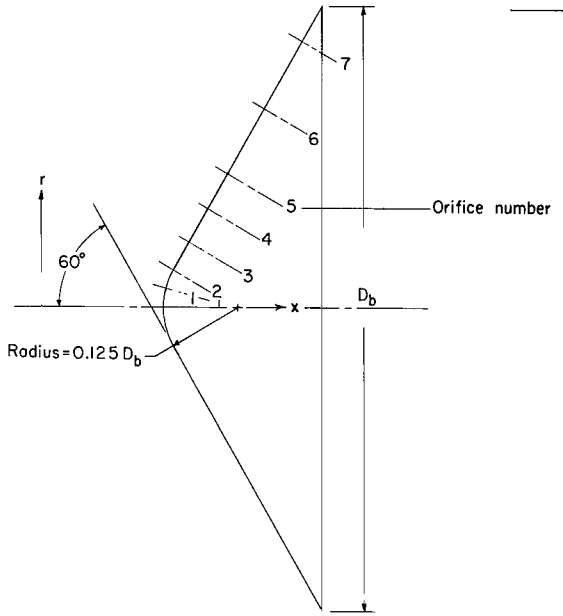

(b) $D_n/D_b = 0.25$.

Figure 1.- Model details and orifice locations. D_b = 11.43 cm.

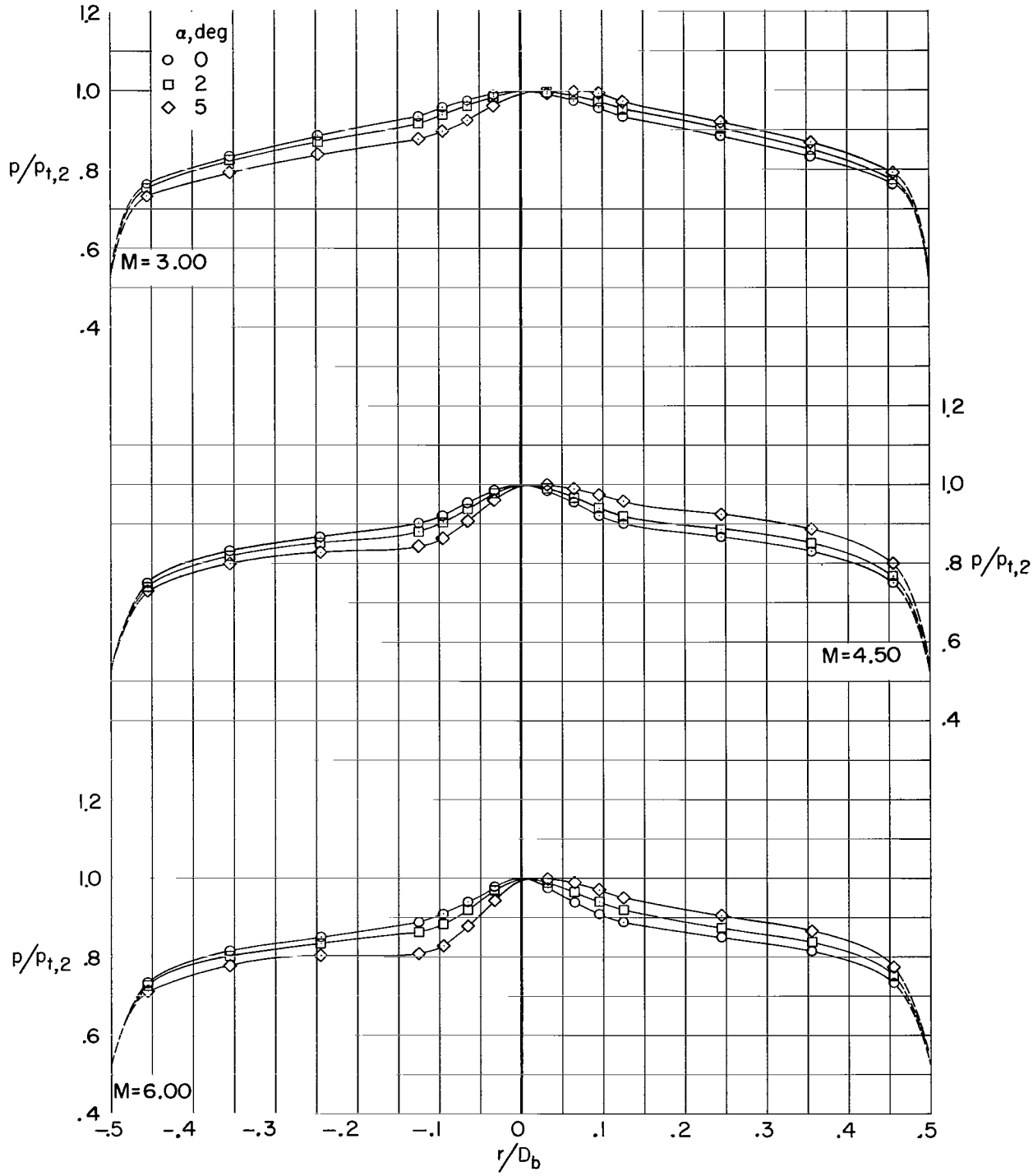

(a) No spike.

Figure 2.- Pressure distributions with varying spike lengths. $D_n/D_b = 0.50$; $d/D_b = 0.0111$; $\theta = 40^0$.

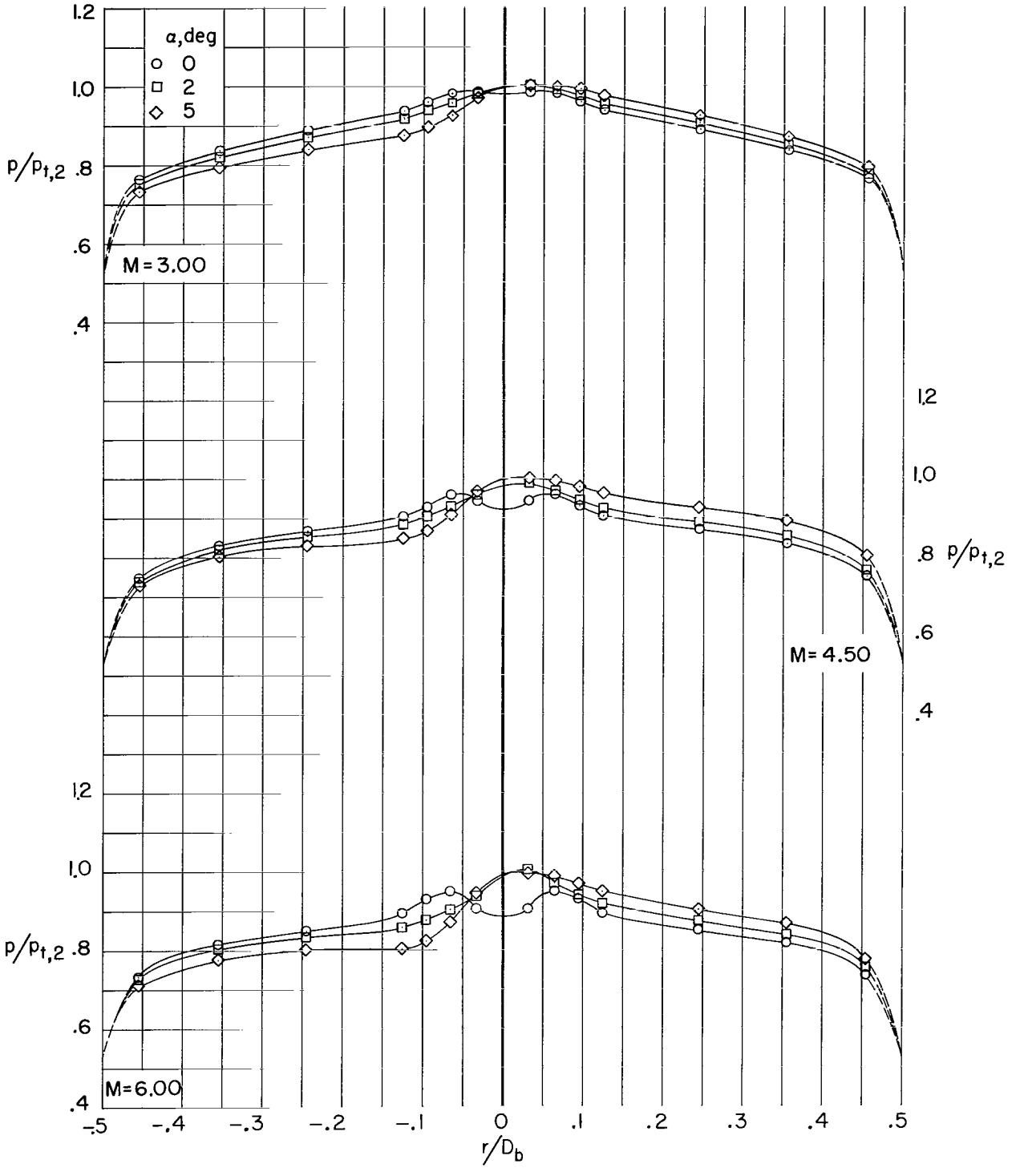

(b) $l/D_b = 0.0489$.

Figure 2.- Continued.

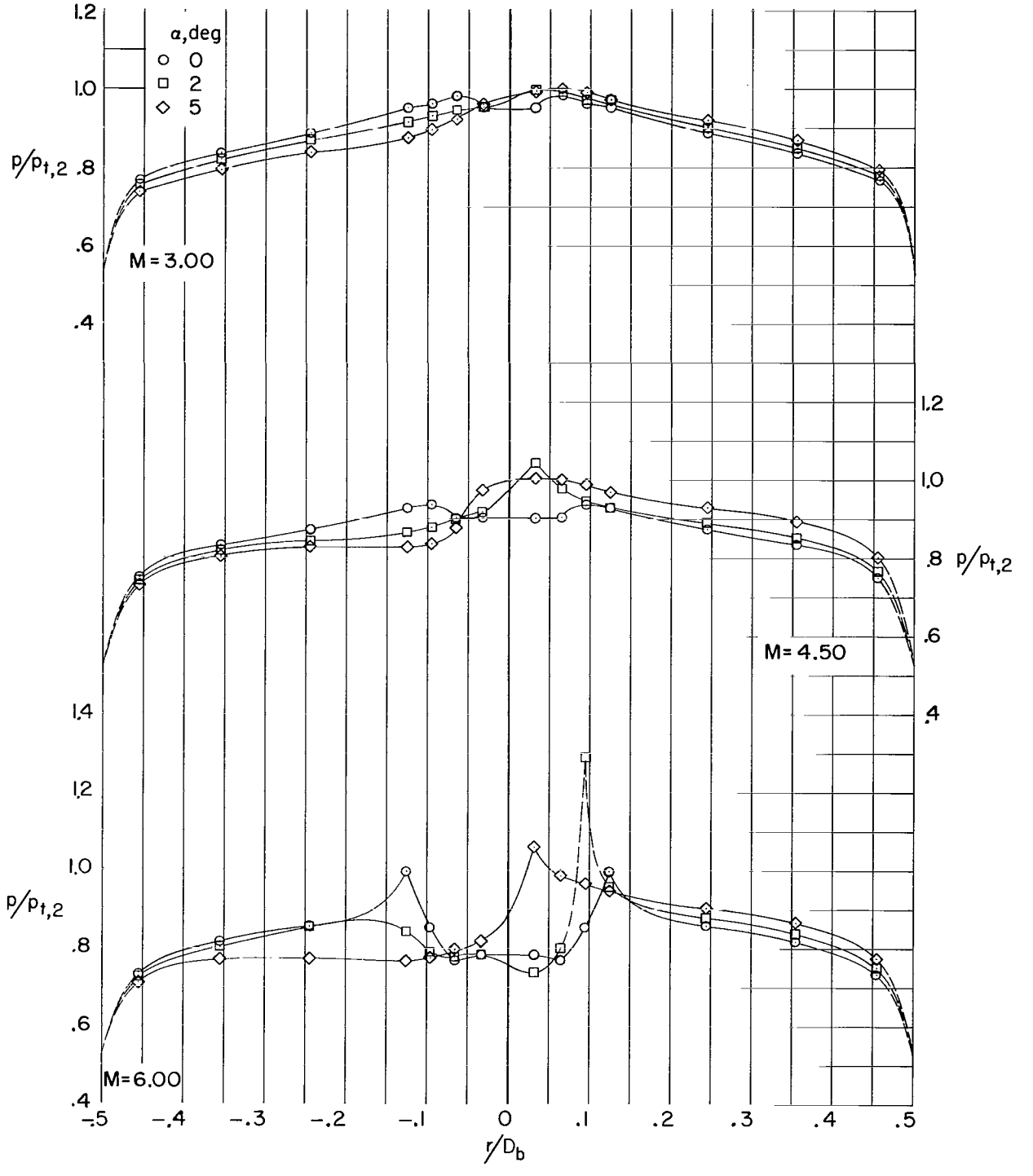

(c) $l/D_b = 0.0767$.

Figure 2.- Continued.

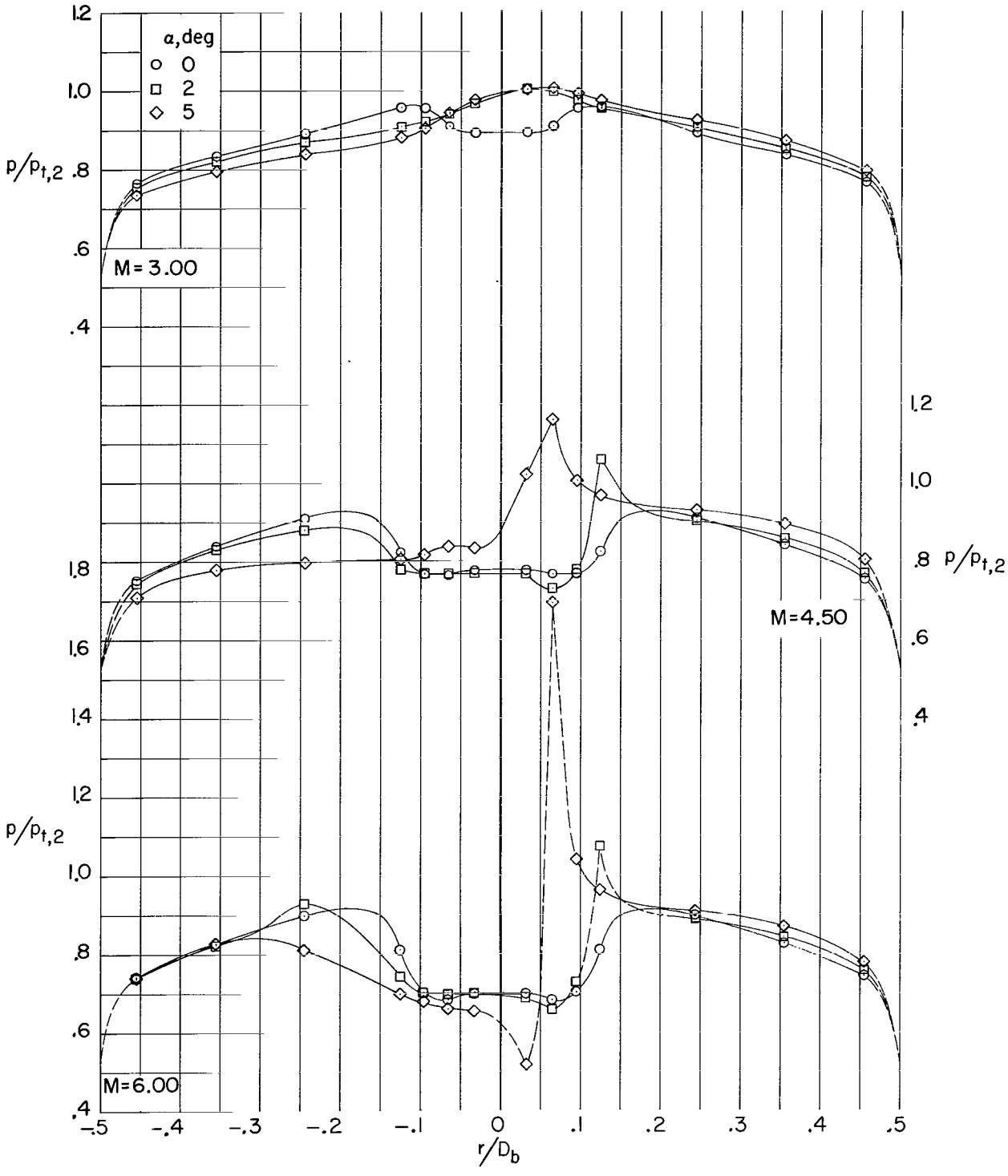

(d) $l/D_b = 0.1045$.

Figure 2.- Continued.

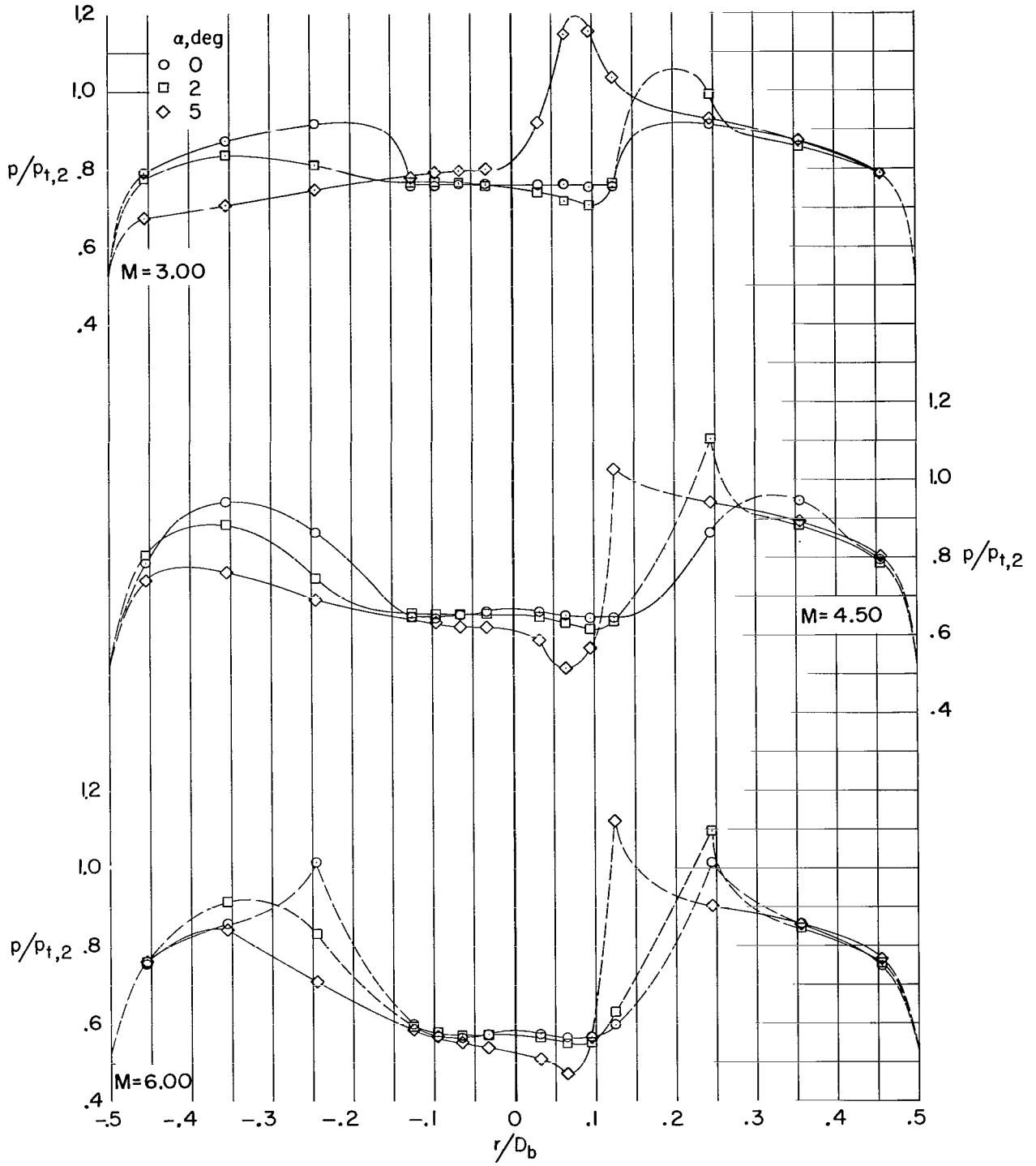

(e) $l/D_b = 0.1601$.

Figure 2.- Continued.

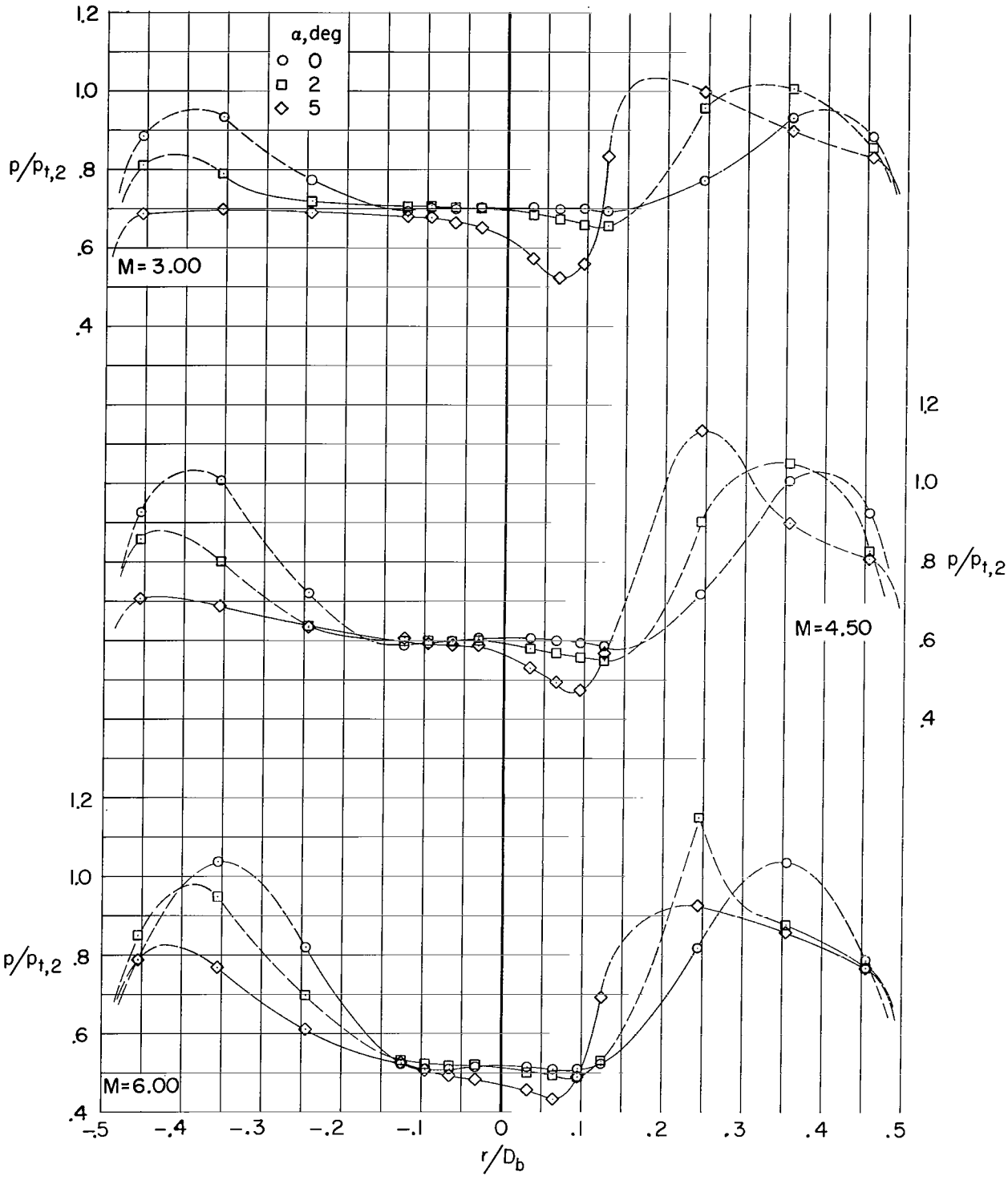

(f) $l/D_b = 0.2156$.

Figure 2.- Concluded.

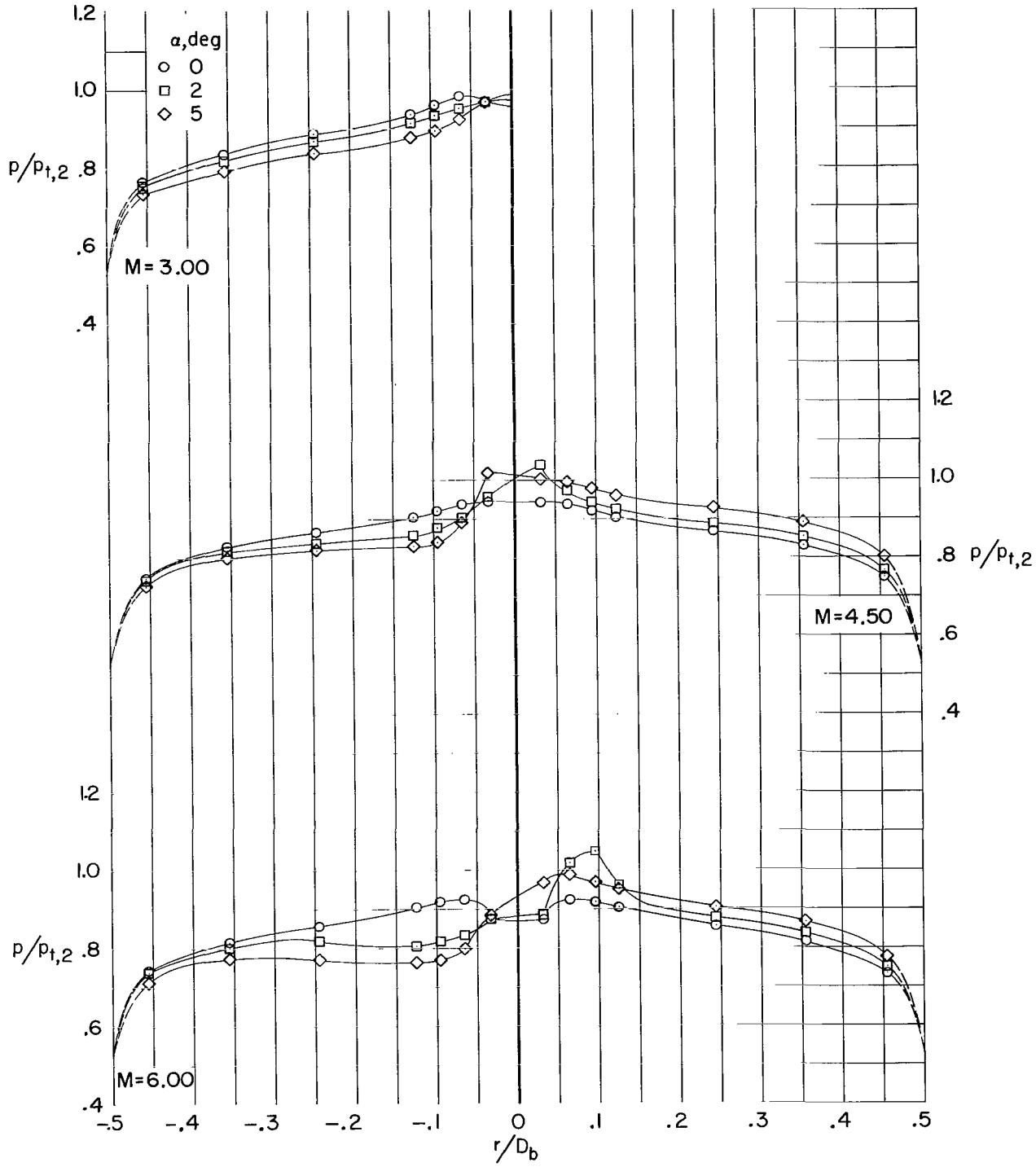

(a) $\theta = 20^0$; $l/D_b = 0.0680$.

Figure 3.- Pressure distributions with varying spike-tip angles. $D_n/D_b = 0.50$; $d/D_b = 0.0111$.

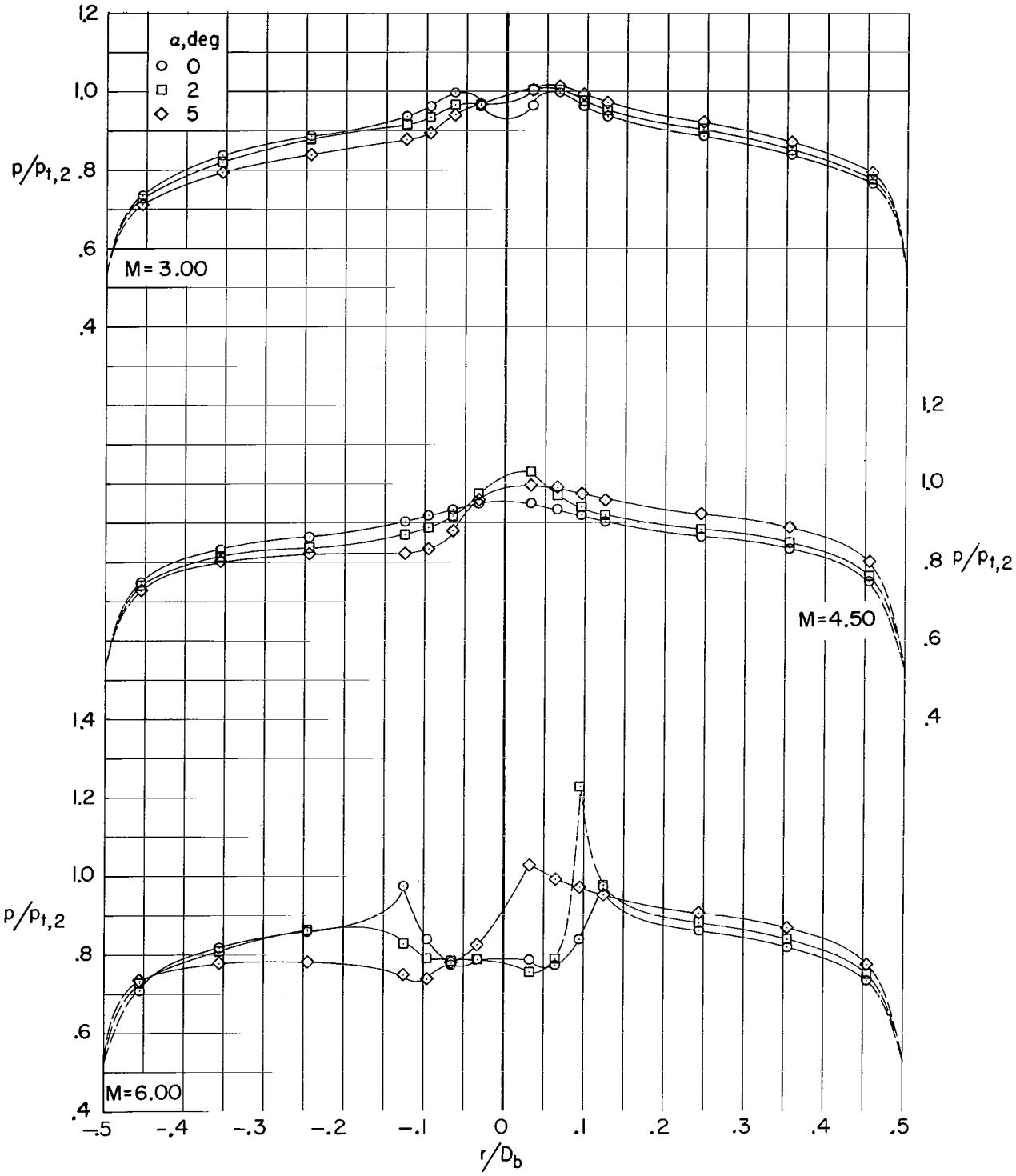

(b) $\theta = 30^0$; $l/D_b = 0.0737$.

Figure 3.- Concluded.

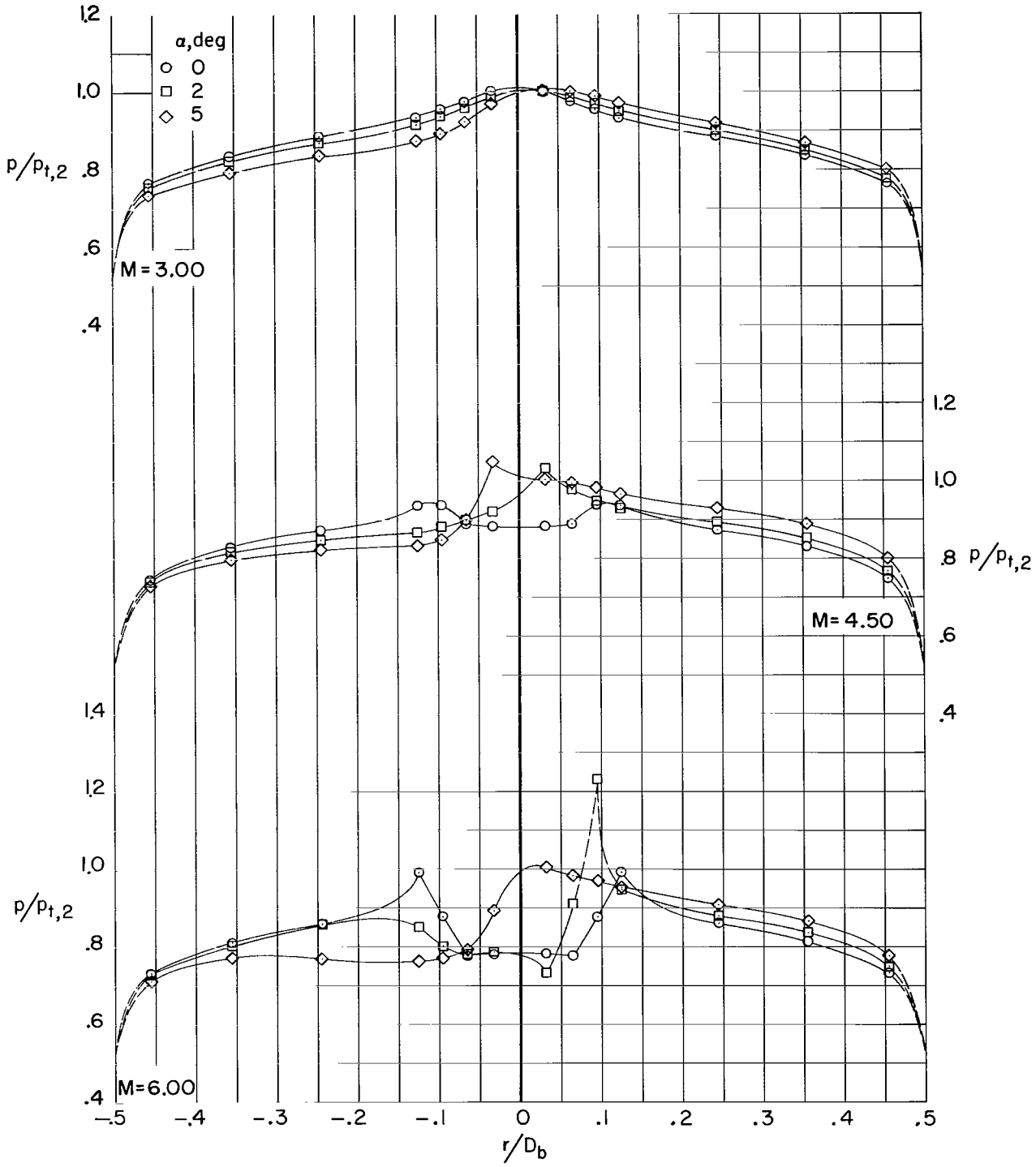

(a) $d/D_b = 0.0044$; $\ell/D_b = 0.0807$.

Figure 4.- Pressure distributions with varying spike diameters. $D_n/D_b = 0.50$; $\theta = 40^0$.

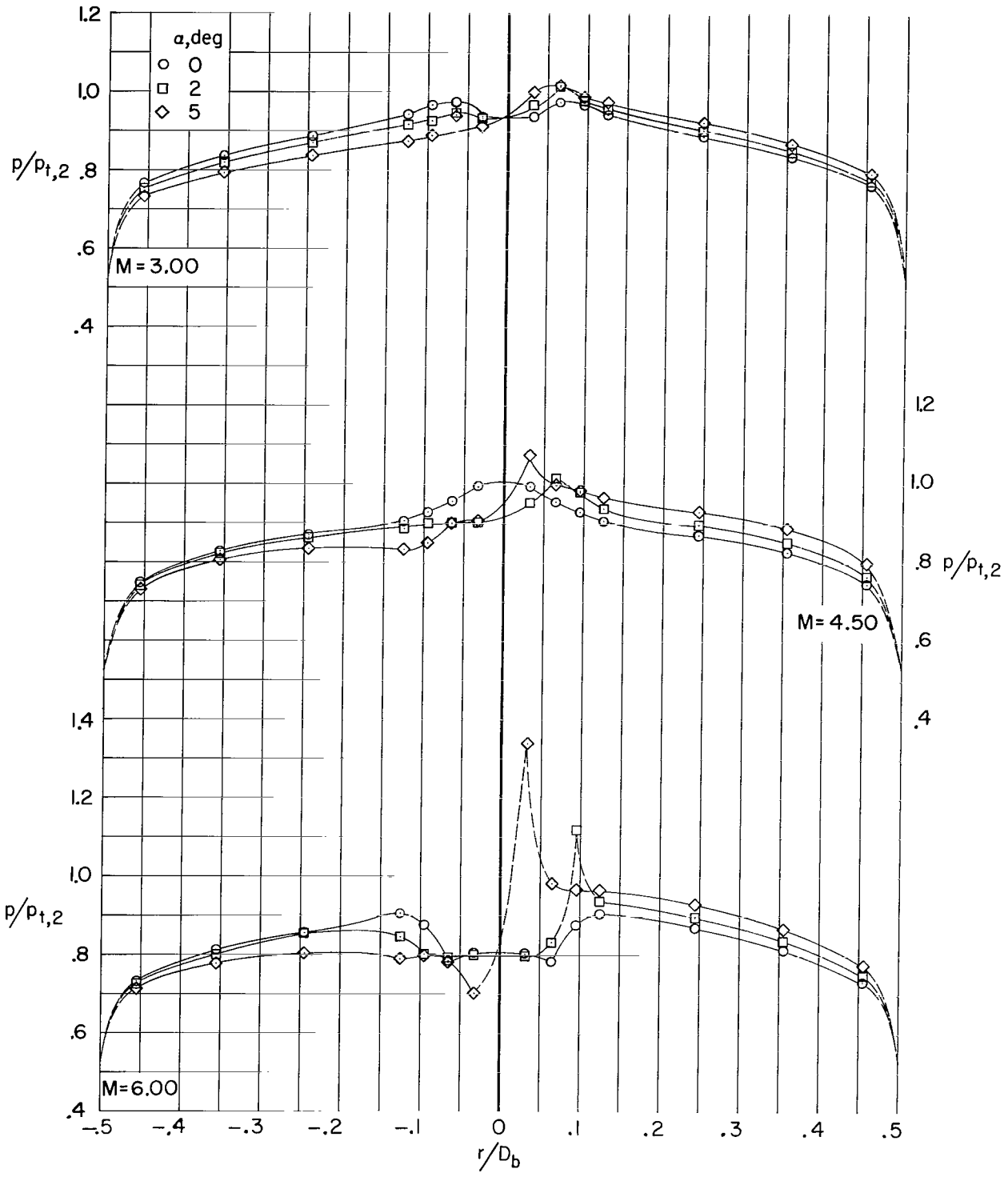

(b) $d/D_b = 0.0444$; $\ell/D_b = 0.0568$.

Figure 4.- Continued.

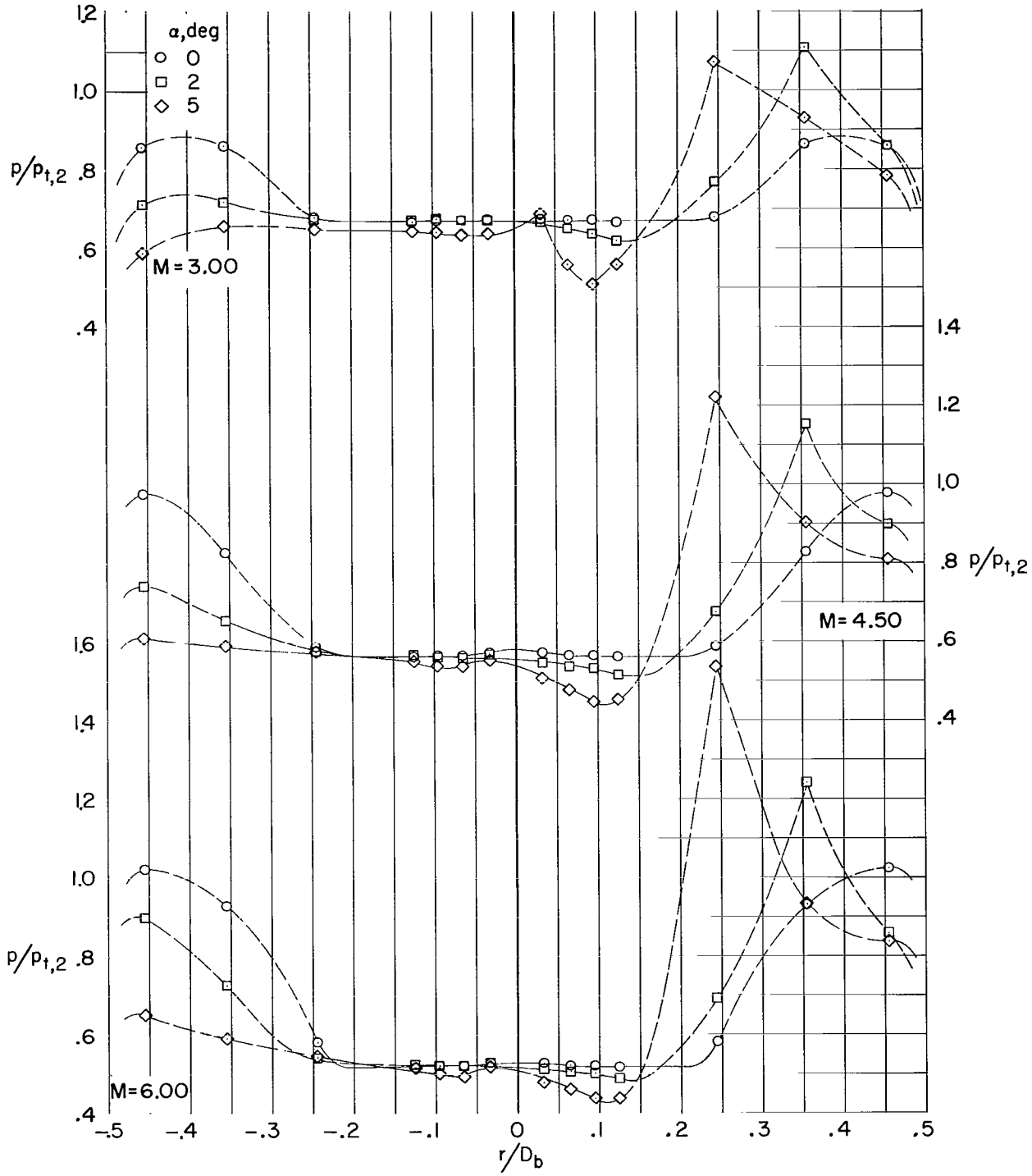

(c) $d/D_b = 0.0555$; $\ell/D_b = 0.1892$.

Figure 4.- Concluded.

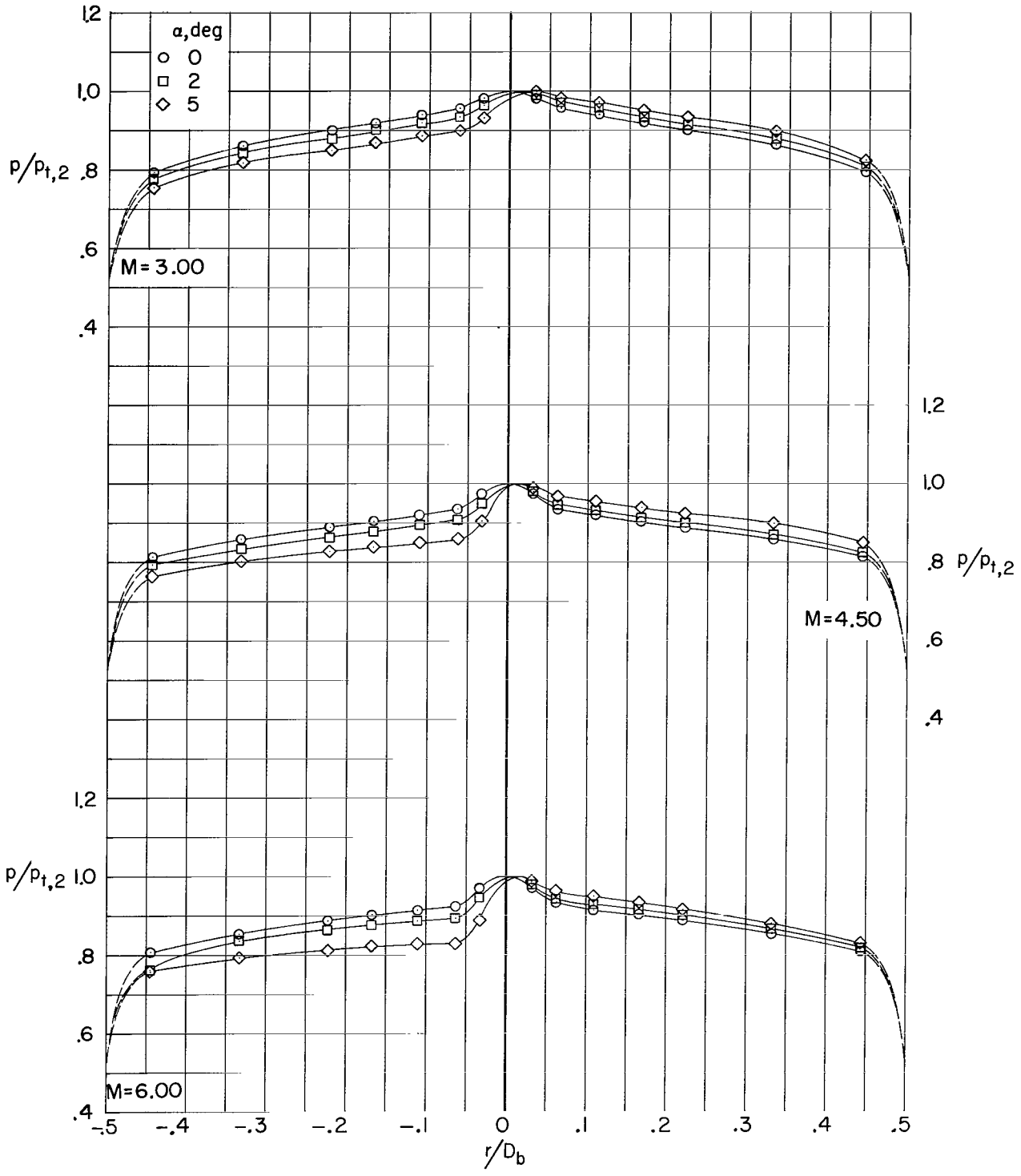

(a) No spike.

Figure 5.- Pressure distributions with varying spike length. $D_n/D_b = 0.25$; $d/D_b = 0.0111$; $\theta = 40^0$.

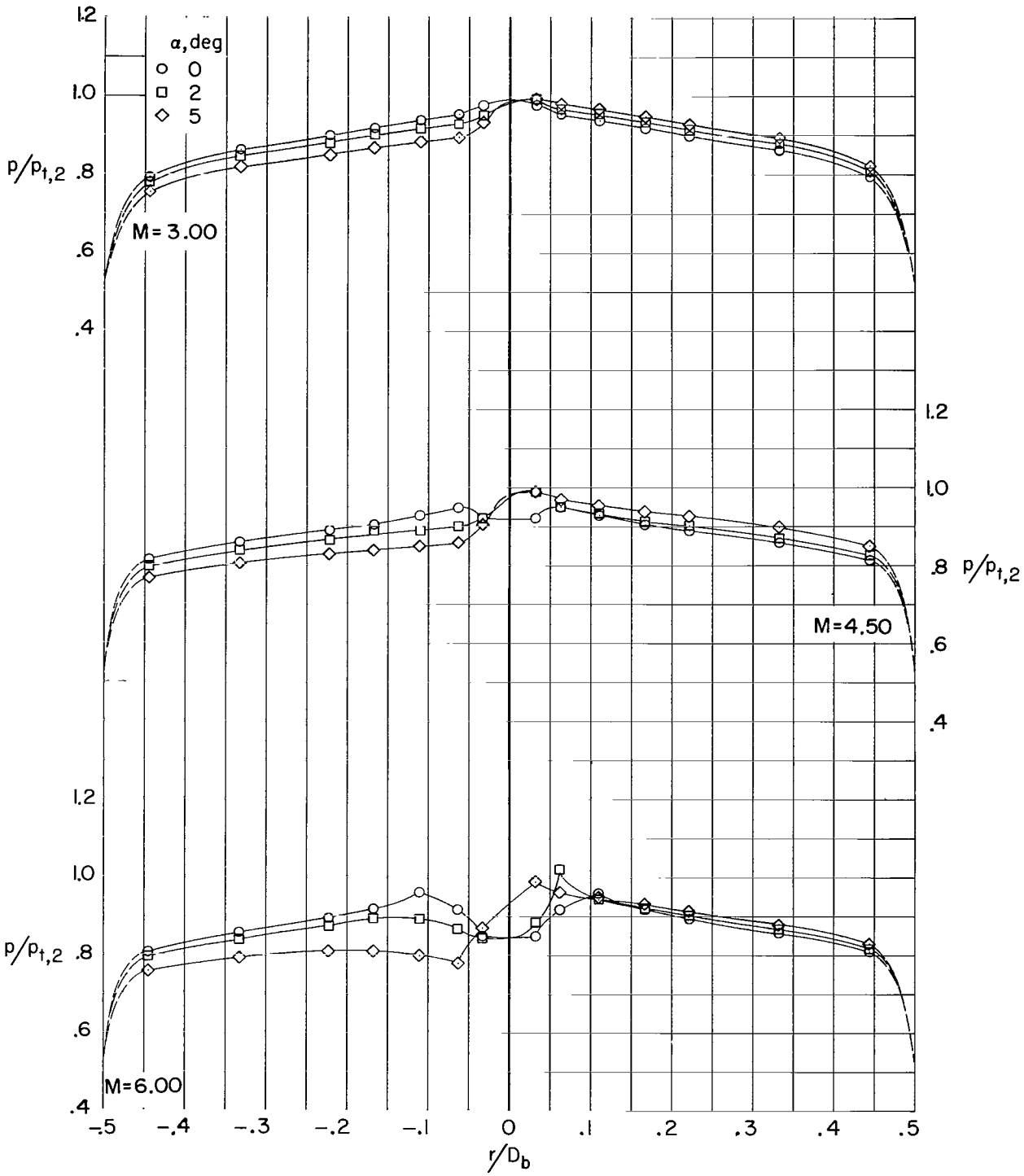

(b) $l/D_b = 0.0489$.

Figure 5.- Continued.

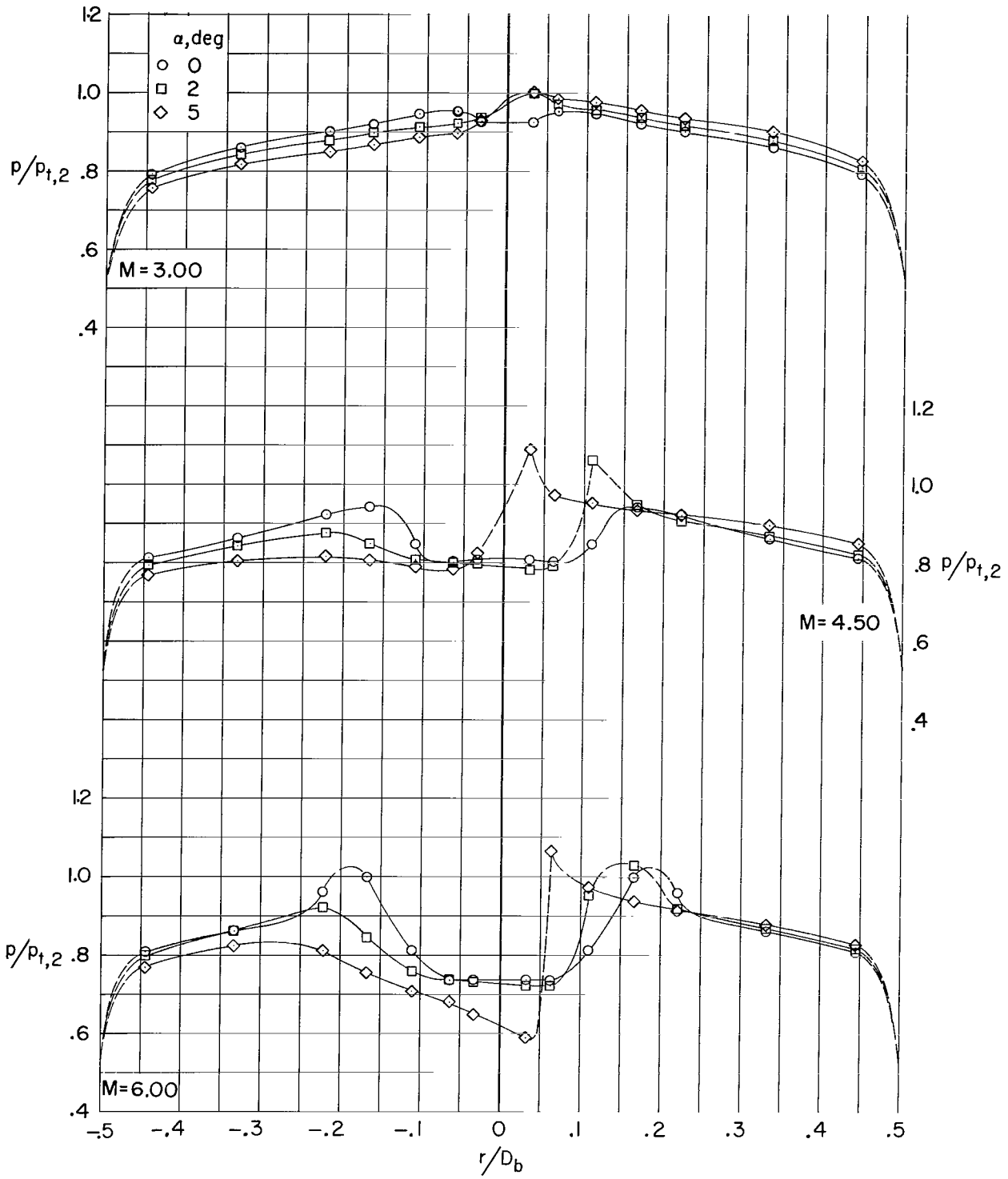

(c) $l/D_b = 0.0767$.

Figure 5.- Concluded.

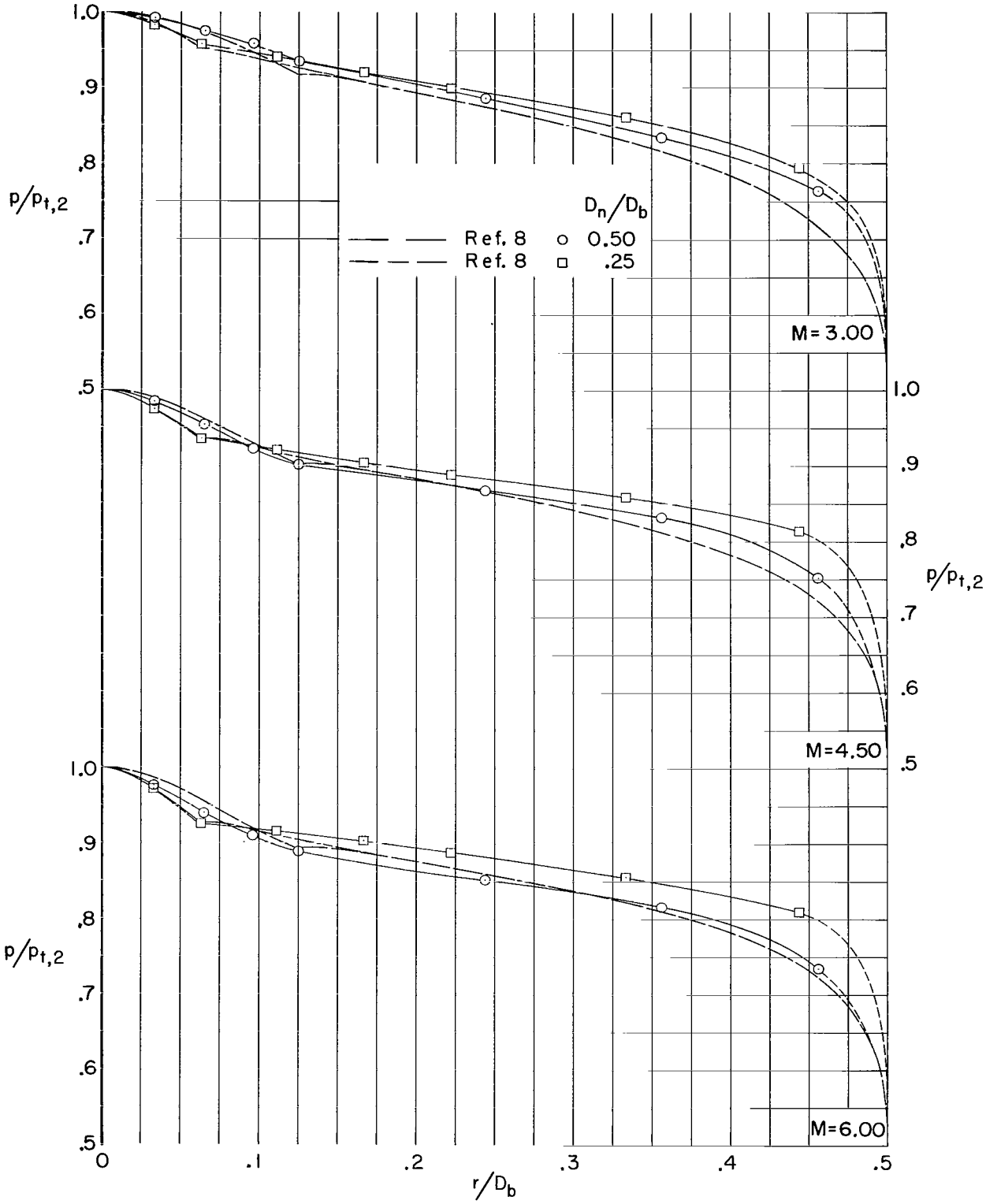

Figure 6.- Effect of nose bluntness D_n/D_b on pressure distributions. No spike; $\alpha = 0^o$.

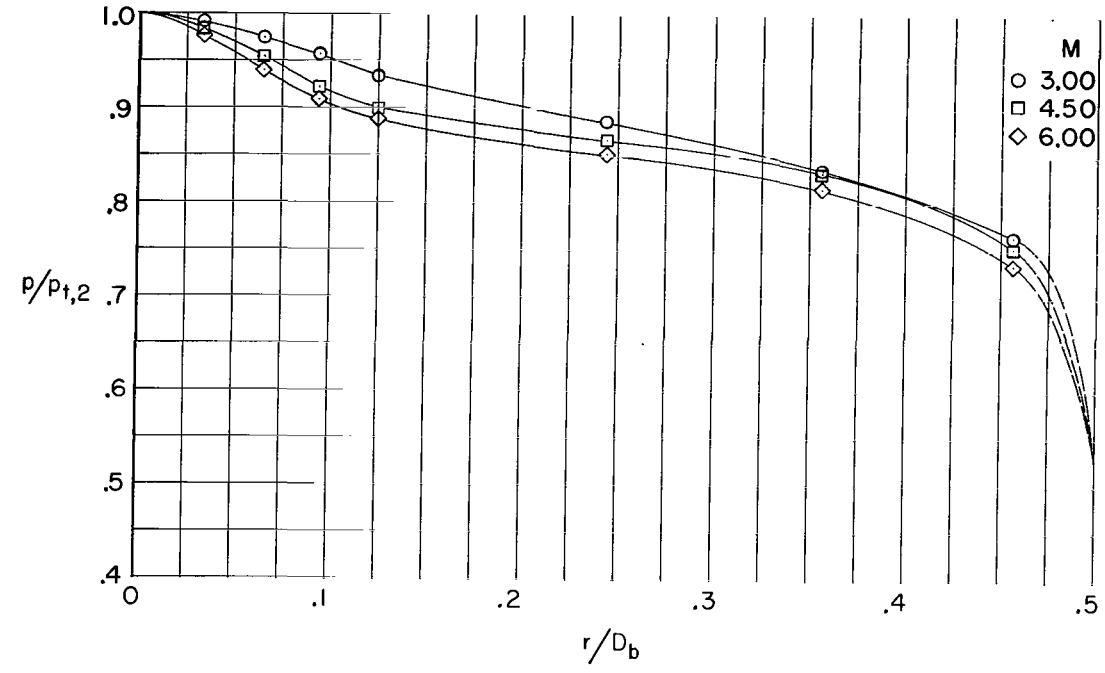

(a) $D_n/D_b = 0.50$.

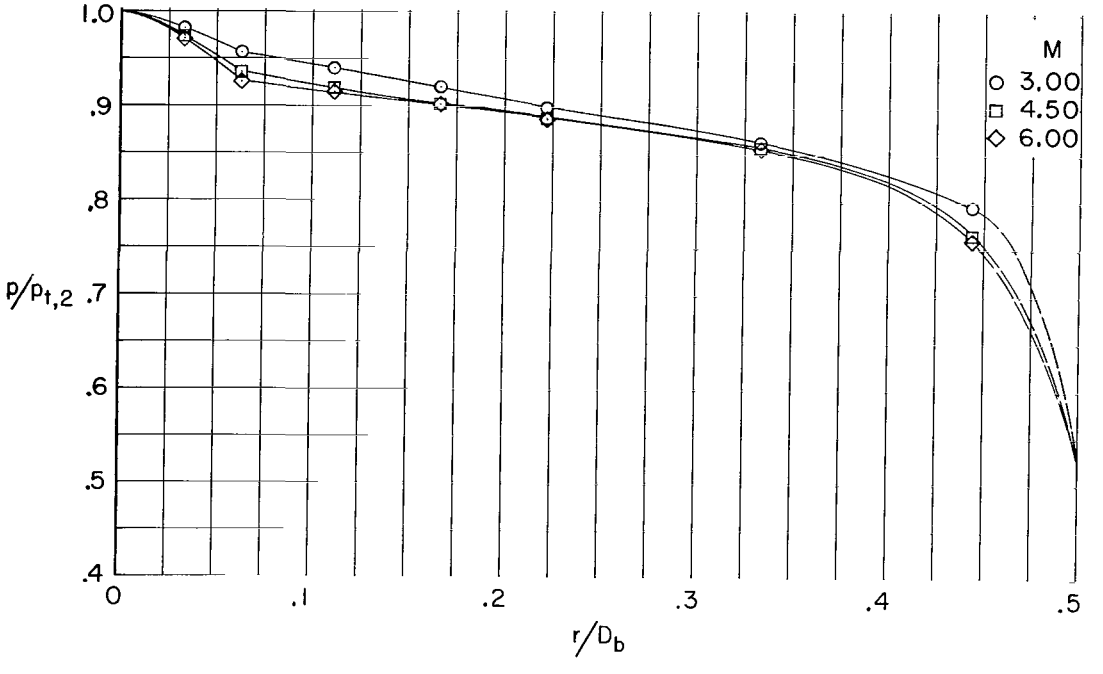

(b) $D_n/D_b = 0.25$.

Figure 7.- Effect of Mach number on pressure distribution. No spike; $\alpha = 0^0$.

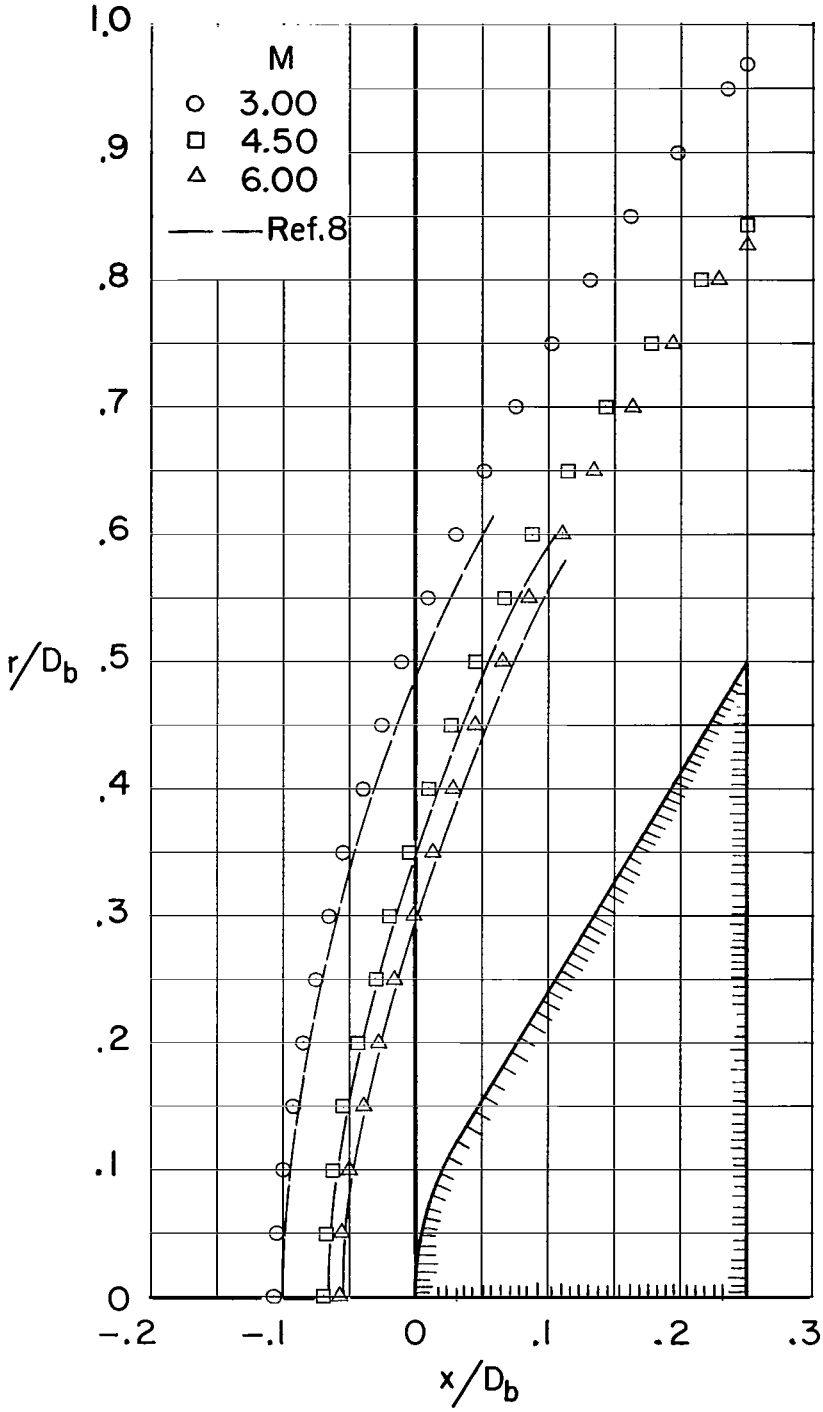

(a) $D_n/D_b = 0.50$.

Figure 8.- Shock shape as a function of Mach number. $\alpha = 0^0$.

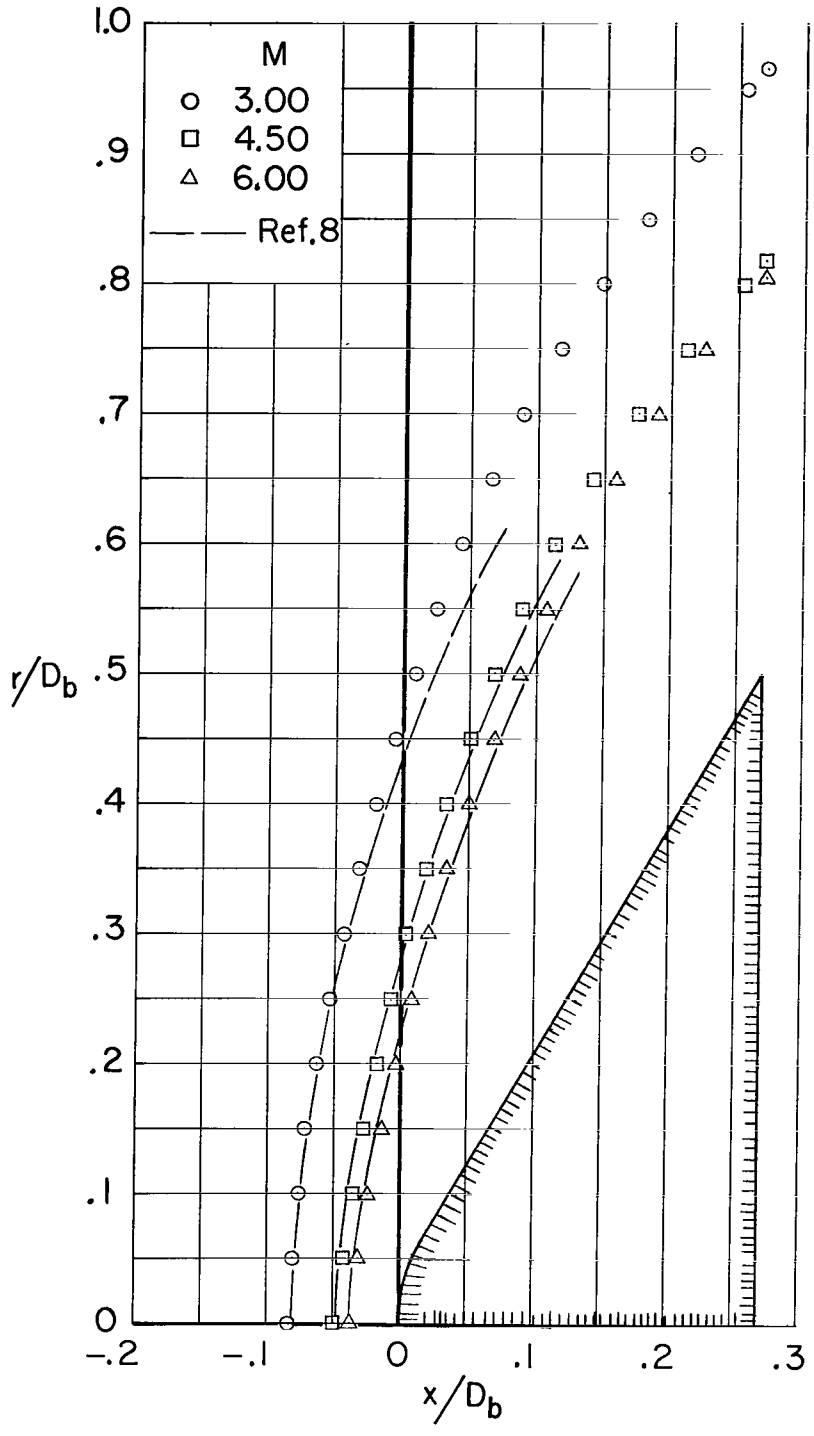

(b) $D_n/D_b = 0.25$.

Figure 8.- Concluded.

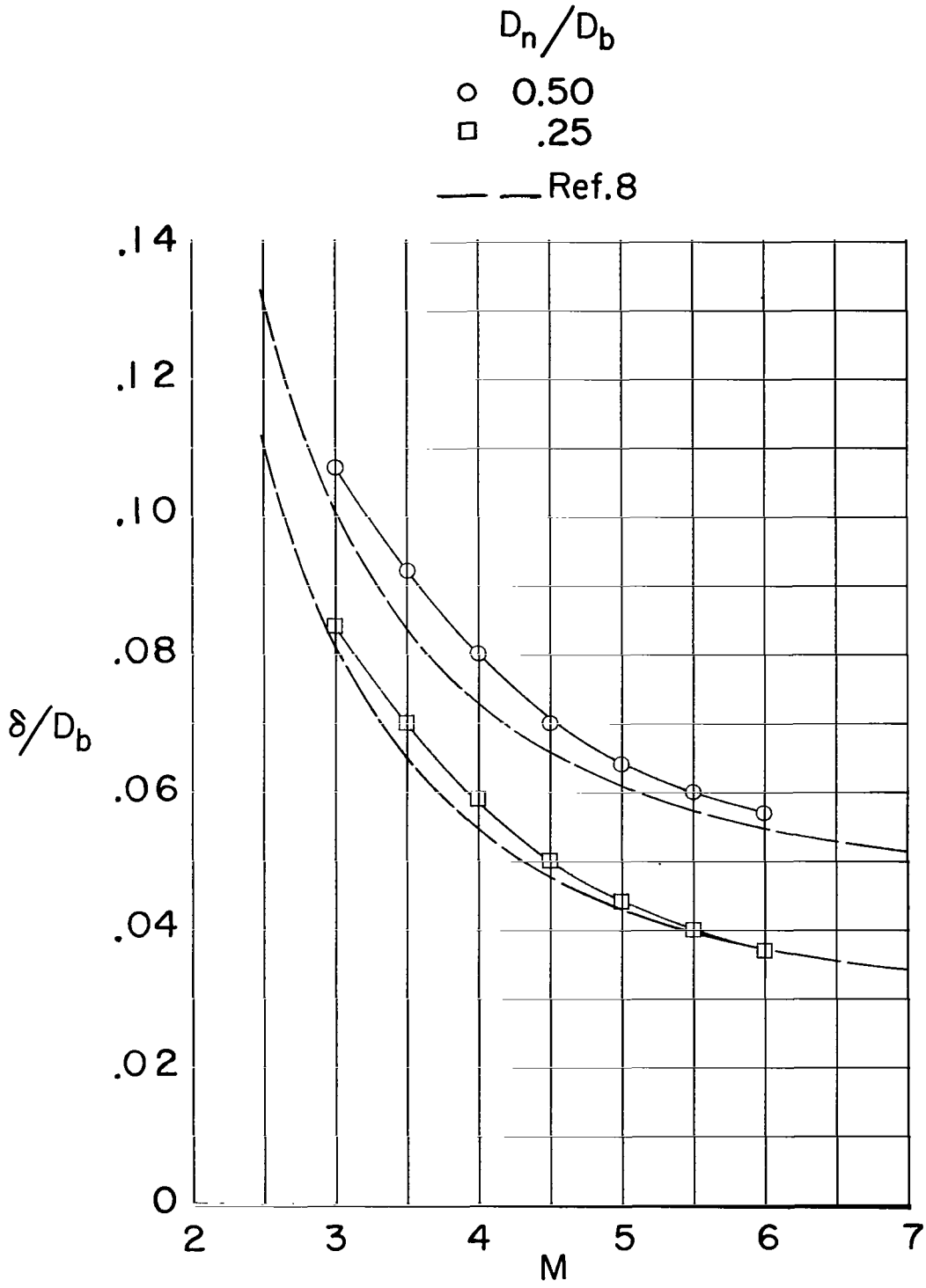

Figure 9.- Bow-shock standoff distance as a function of Mach number. $\alpha = 0^0$.

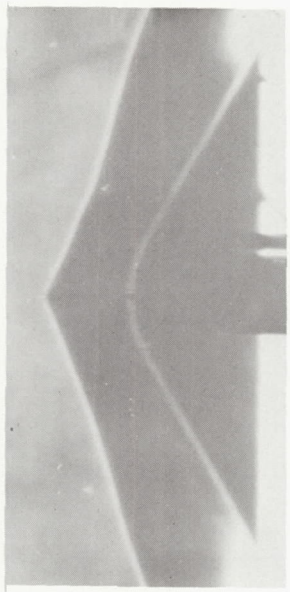

M = 3.00 ; α = 0°

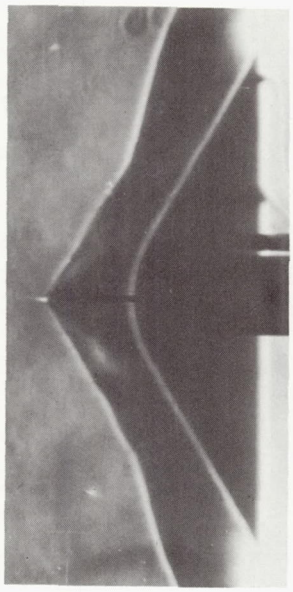

M = 4.50 ; α = 0°

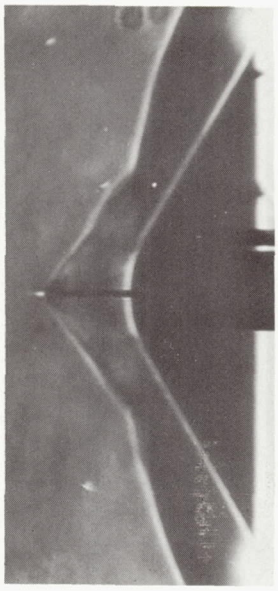

M = 6.00 ; α = 0°

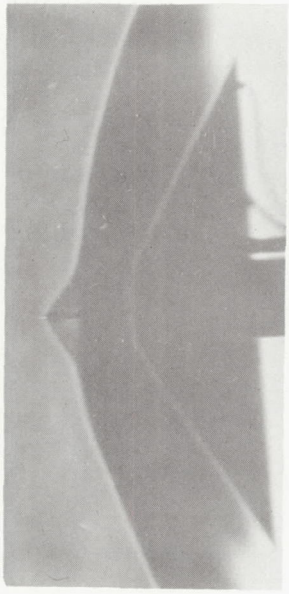

M = 3.00 ; α = 5°

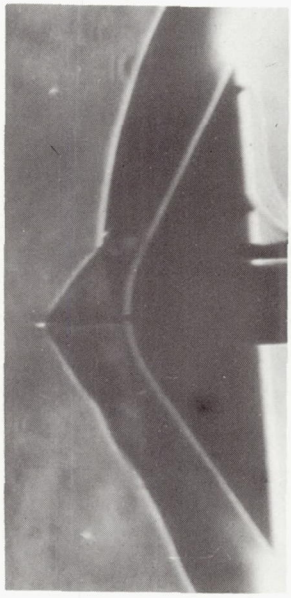

M = 4.50 ; α = 5°

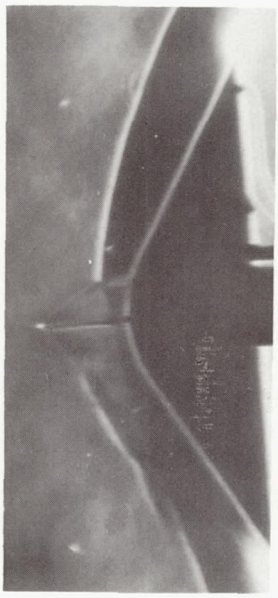

M = 6.00 ; α = 5°

(a) $D_n/D_b = 0.50$; $l/D_b = 0.1601$. L-69-1348

Figure 10.- Typical schlieren photographs of spiked configurations. $d/D_b = 0.0111$; $\theta = 40^0$.

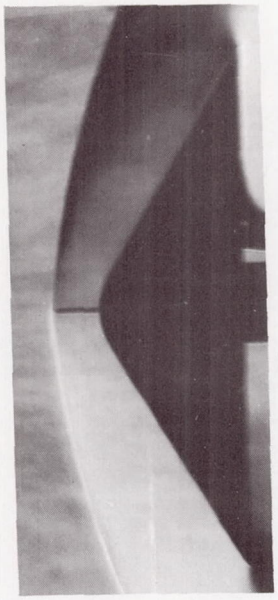

M=3.00 ; α = 0°

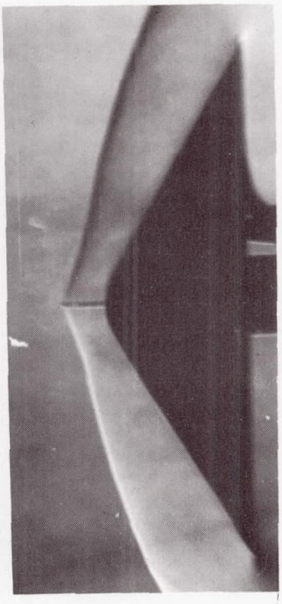

M = 4.50 ; α = 0°

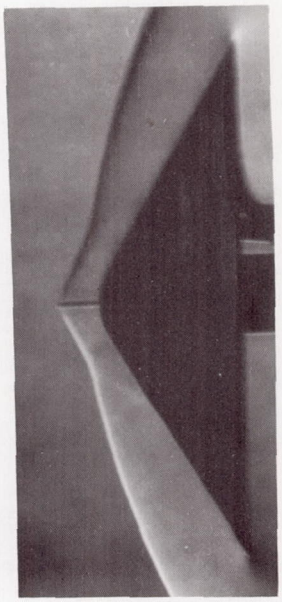

M = 6.00 ; α = 0°

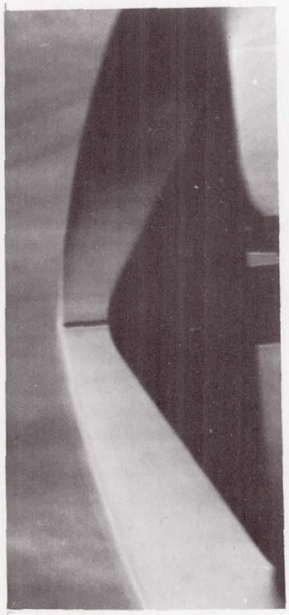

M = 3.00 ; α = 5°

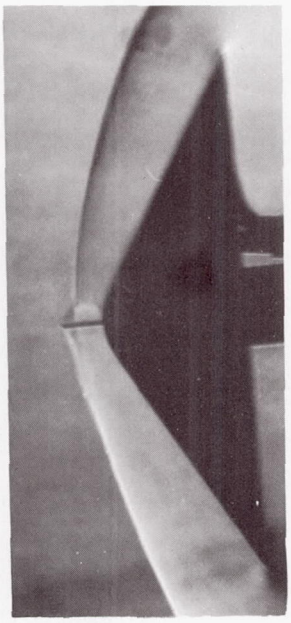

M = 4.50 ; α = 5°

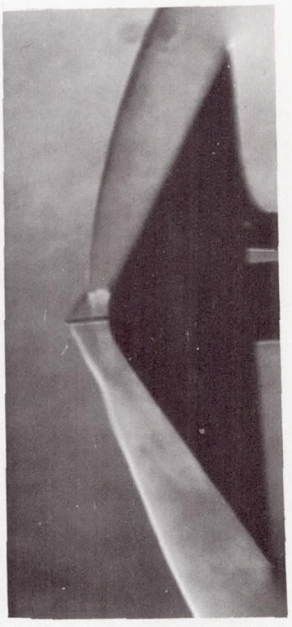

M = 6.00 ; α = 5°

(b) D_n/D_b = 0.25; l/D_b = 0.0767.

L-69-1349

Figure 10.- Concluded.

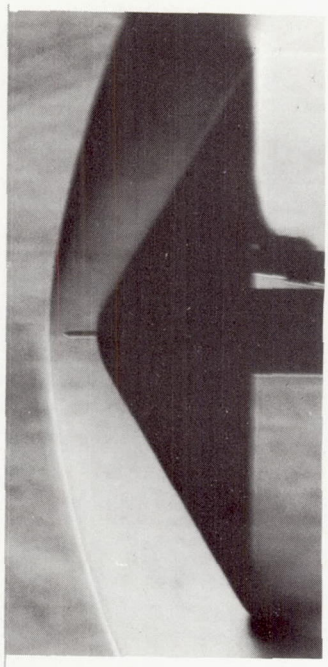

(a) Steady detached bow shock. $l/\delta < 0.8$.

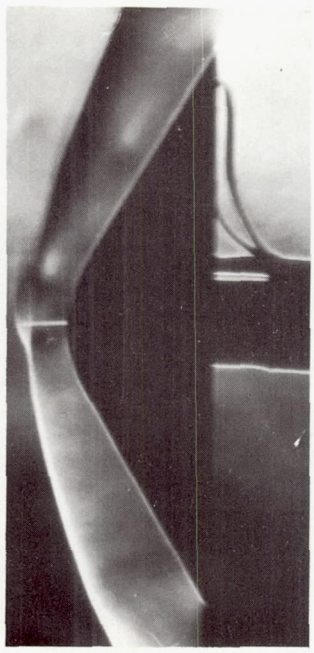

(b) Unsteady detached bow shock. $0.8 < l/\delta < 1.0$.

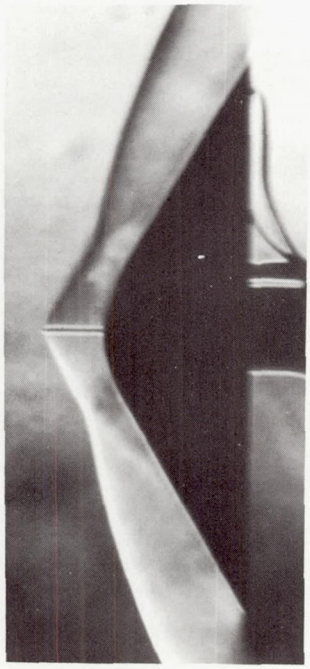

(c) Steady attached bow shock. $1.1 < l/\delta < 2.2$.

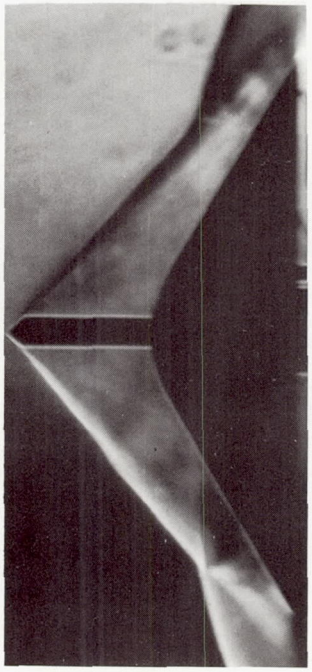

(d) Unsteady attached bow shock. $l/\delta > 2.2$.

L-69-1350

Figure 11.- Typical schlieren photographs which illustrate the types of flow that occurred in the vicinity of the spikes. $\alpha = 0^{0}$.

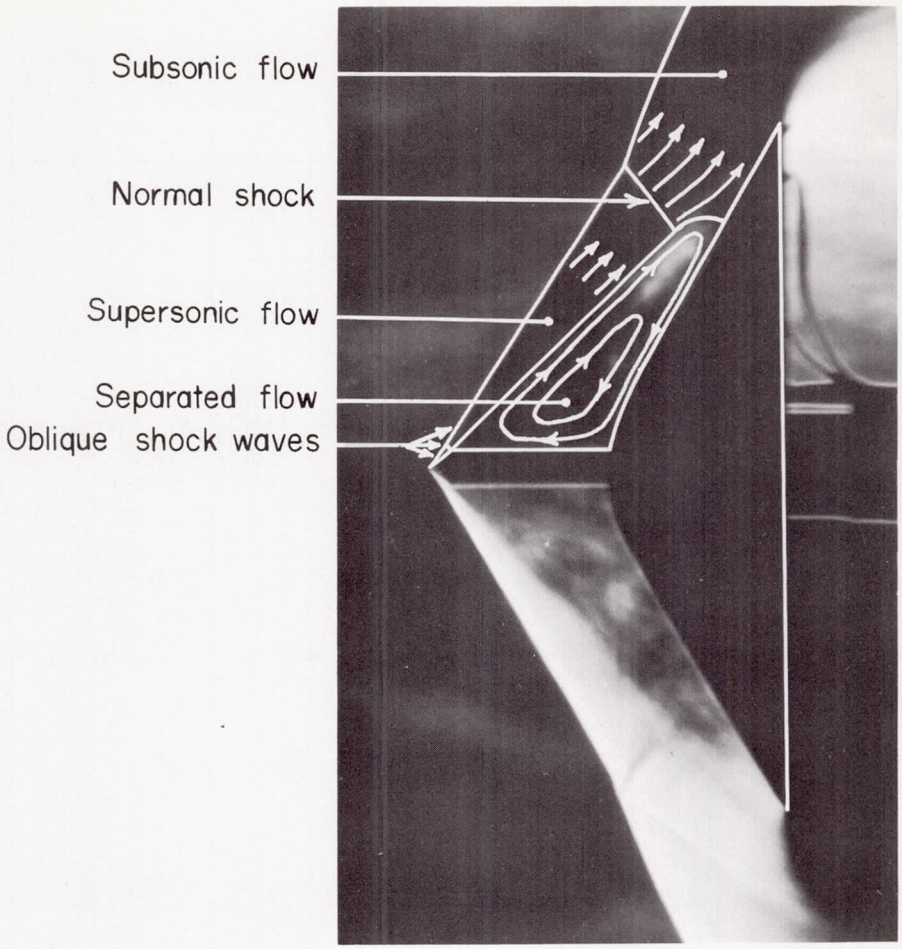

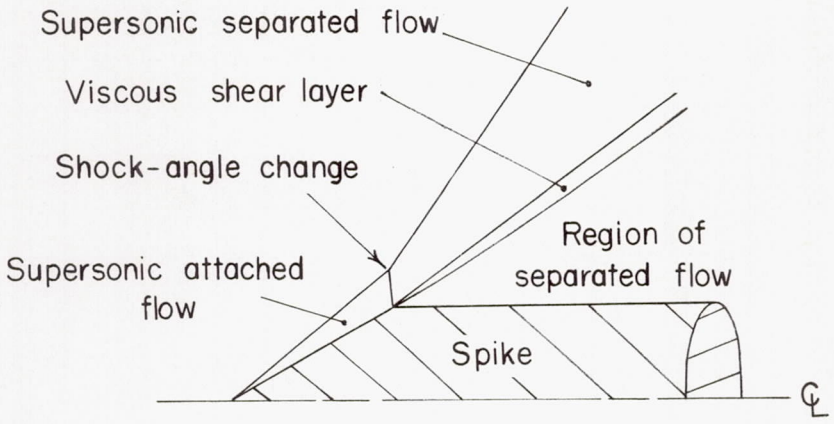

Figure 12.- Flow phenomena induced by a long large-diameter spike. $\alpha = 0^{0}$.

L-69-1351

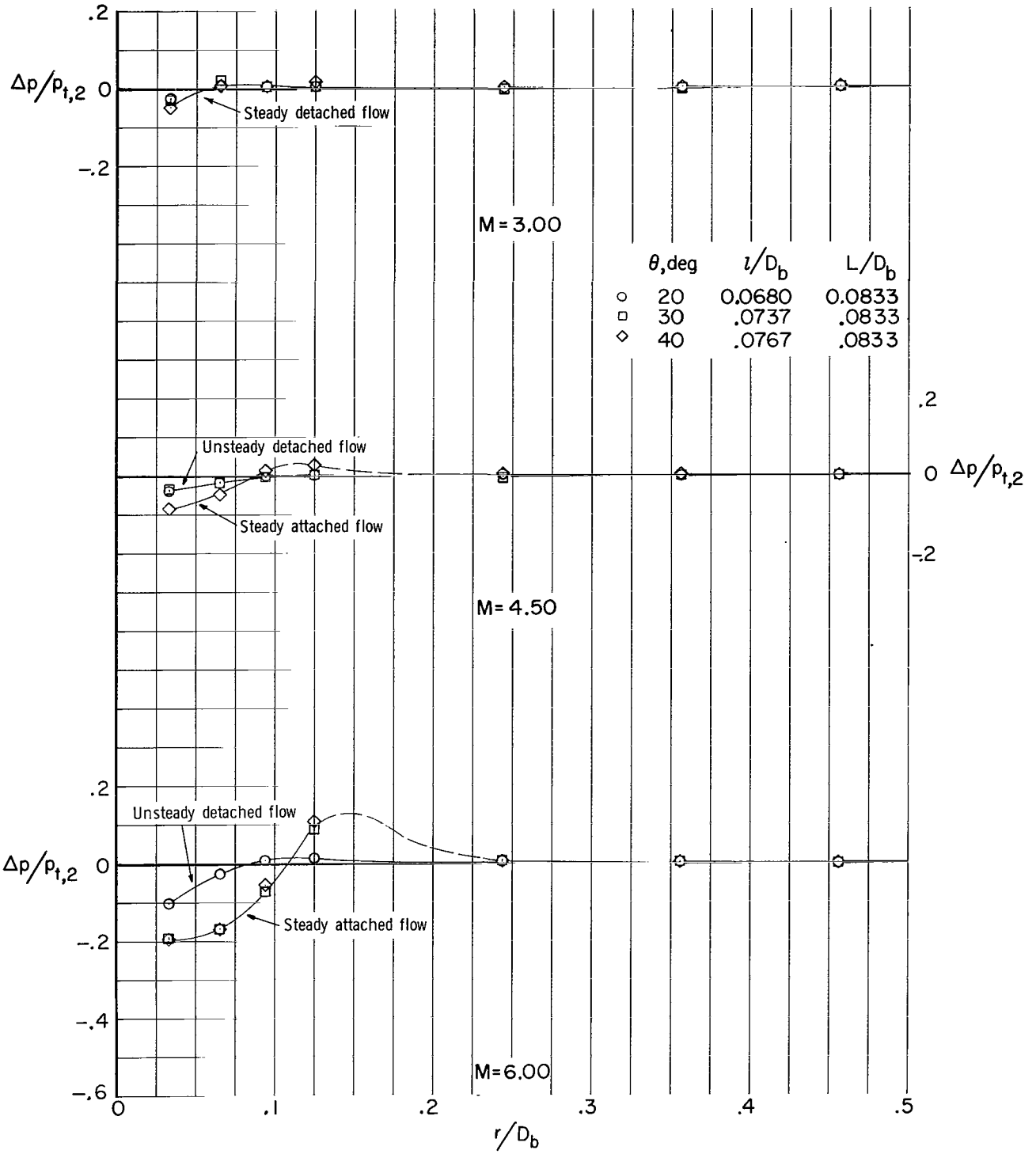

Figure 13.- Change in pressure distribution due to spike-tip angle. $\alpha = 0^0$; $D_n/D_b = 0.50$; $d/D_b = 0.0111$.

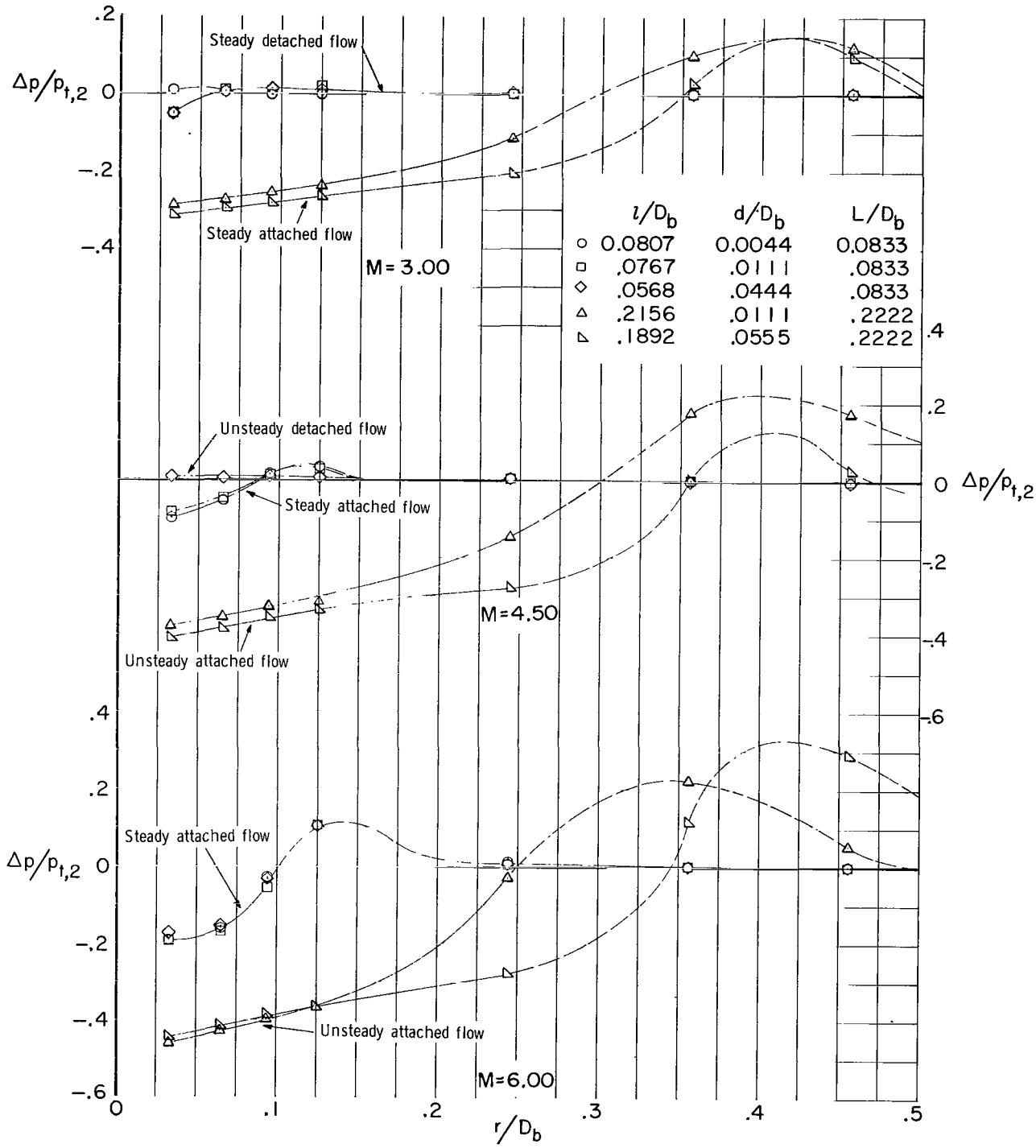

Figure 14.- Change in pressure distribution due to spike diameter. $\alpha = 0^0$; $D_n/D_b = 0.50$; $\theta = 40^0$.

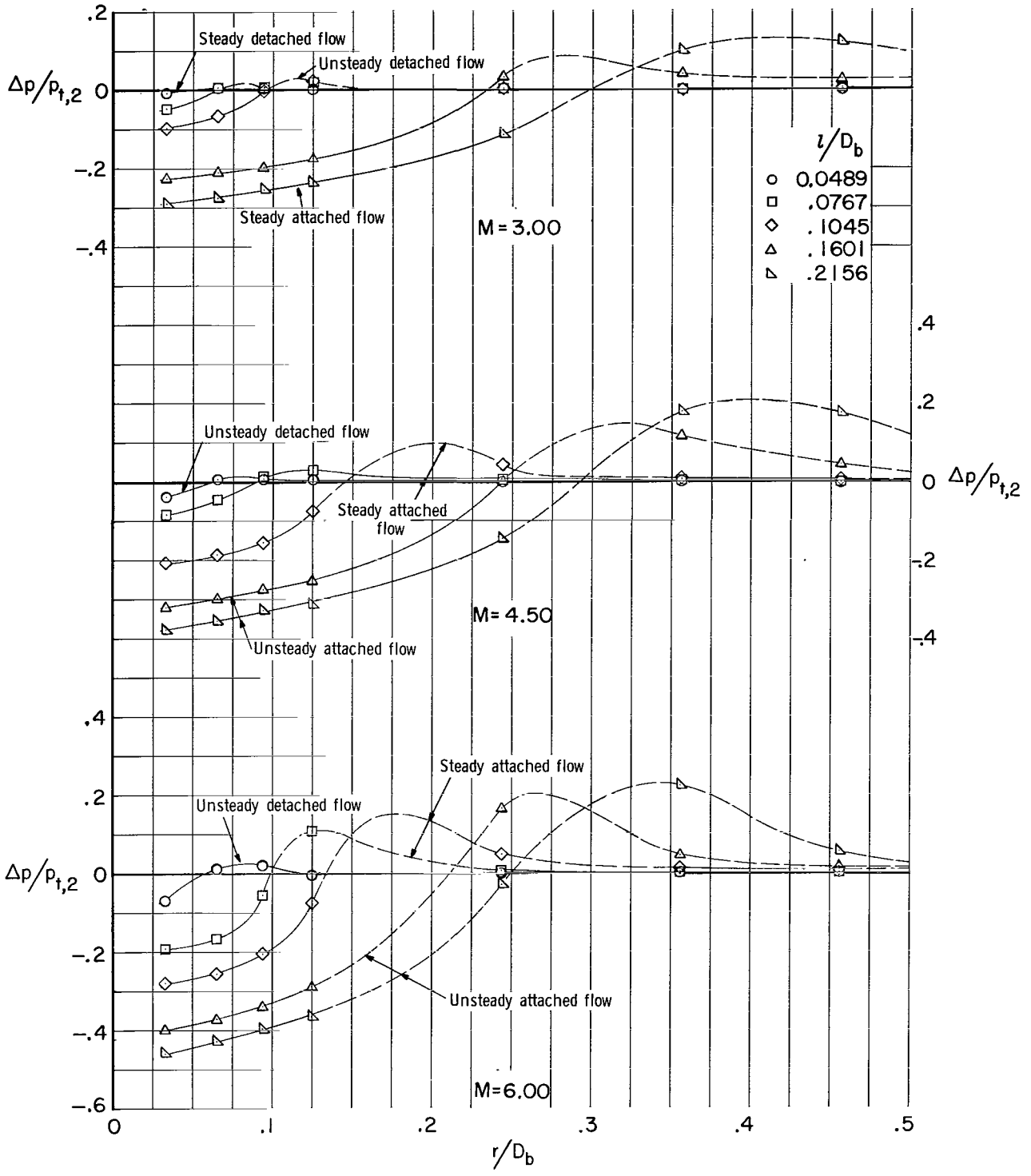

(a) $D_n/D_b = 0.50$.

Figure 15.- Change in pressure distribution due to spike length. $\alpha = 0^0$; $d/D_b = 0.0111$; $\theta = 40^0$.

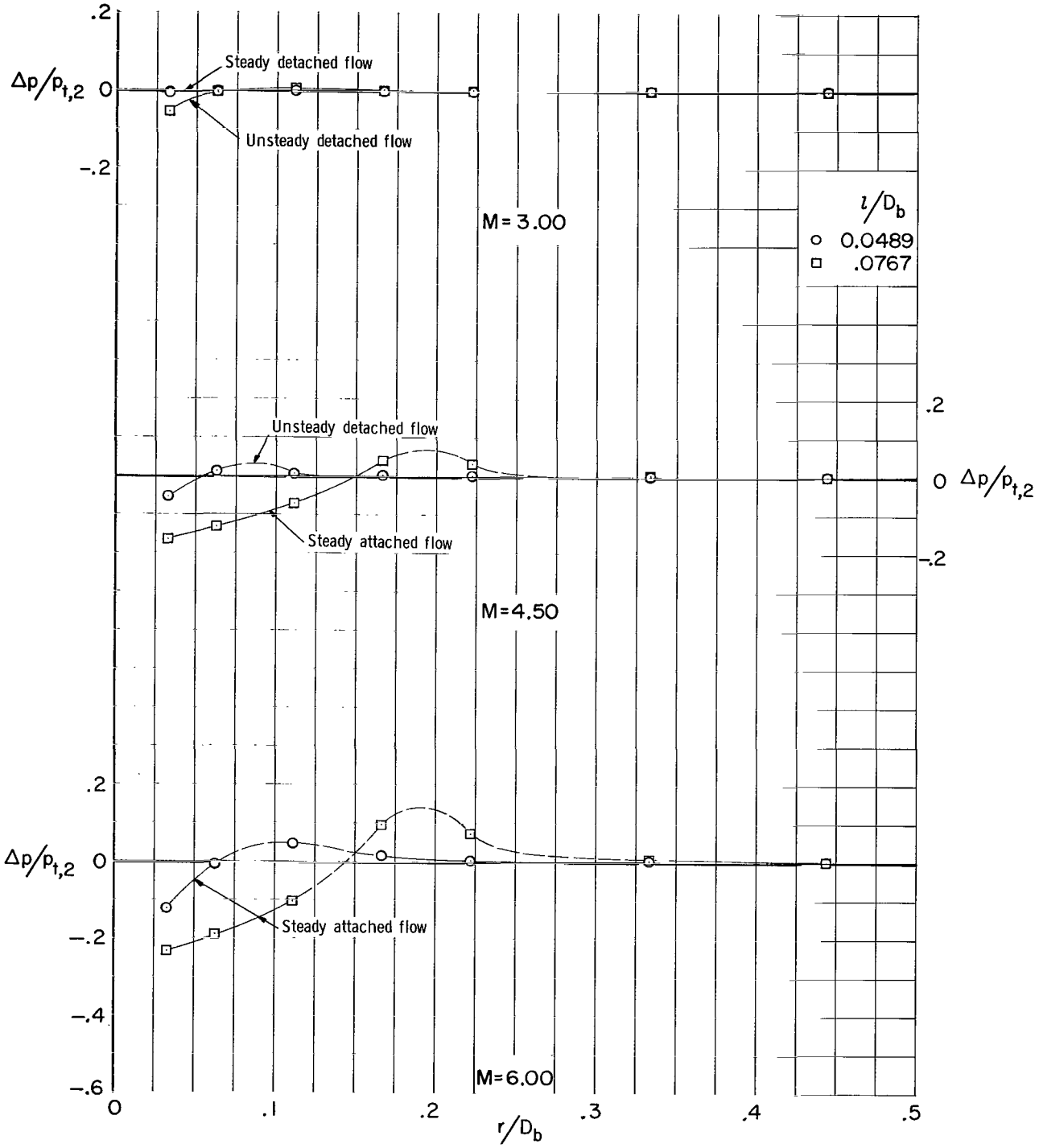

(b) $D_n/D_b = 0.25$.

Figure 15.- Concluded.

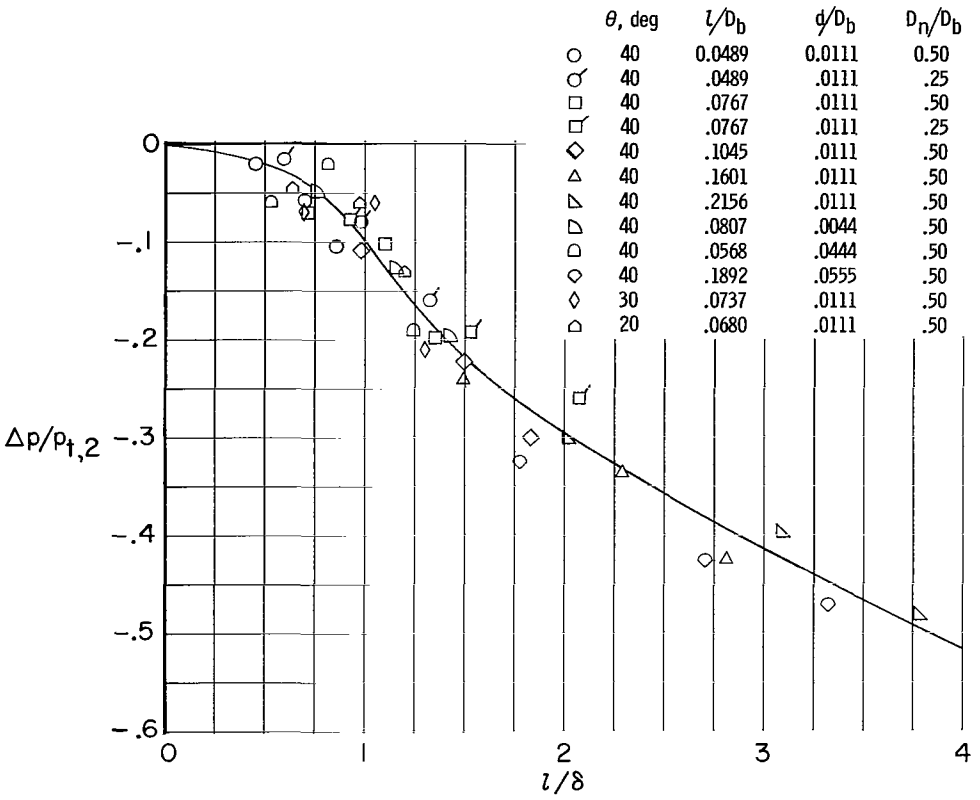

(a) Separation pressure at $r/D_b = d/2D_b$.

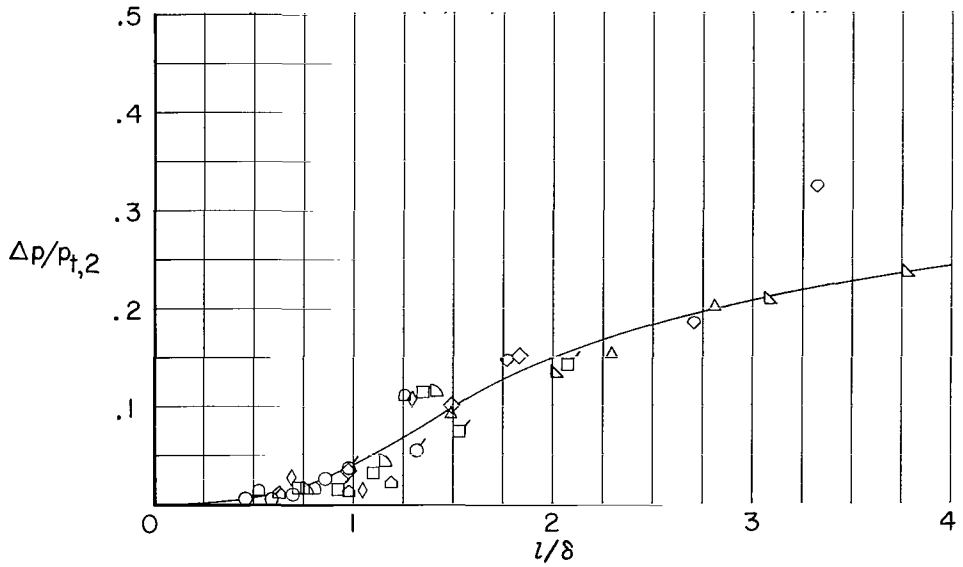

(b) Maximum pressure at flow reattachment.

Figure 16.- Correlation of spike data. $\alpha = 0^0$.

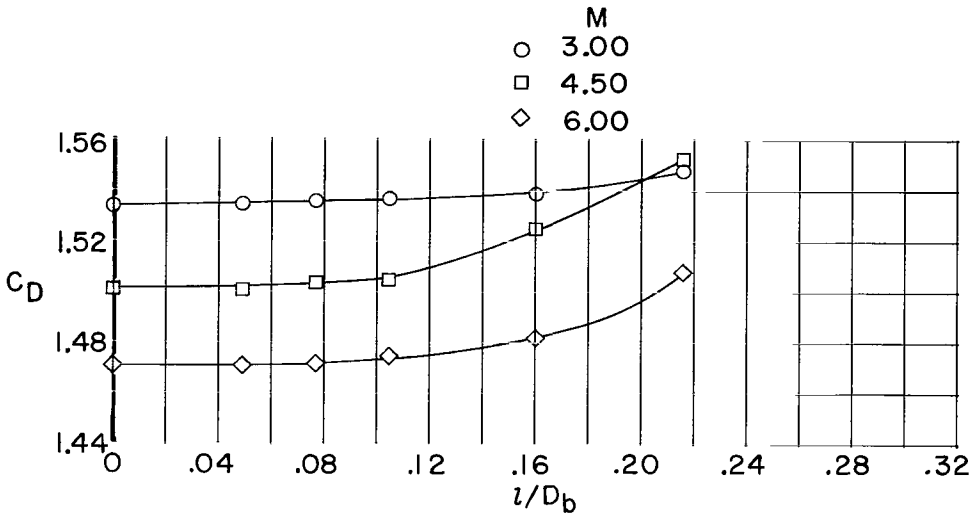

(a) $D_n/D_b = 0.50$.

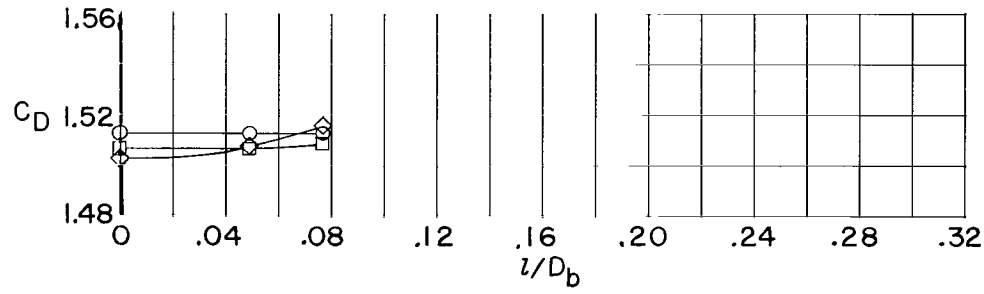

(b) $D_n/D_b = 0.25$.

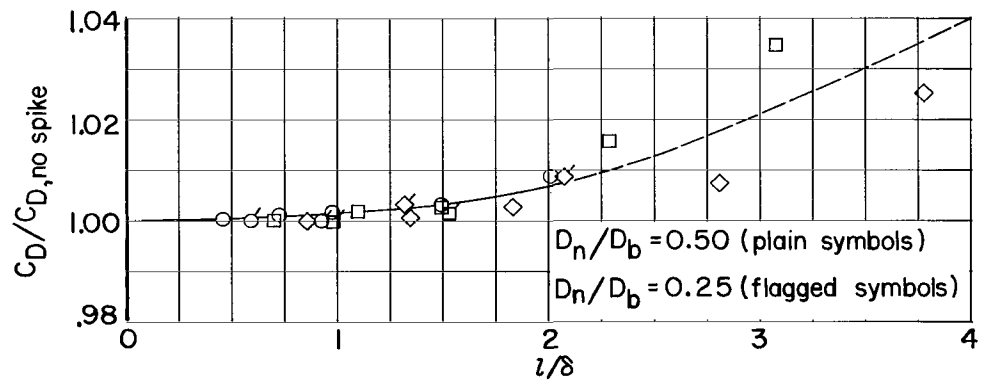

(c) Data correlation.

Figure 17.- Effect of spike-length parameters on the integrated-pressure drag coefficient. $\alpha = 0^0$; $d/D_b = 0.0111$; $\theta = 40^0$.

NATIONAL AERONAUTICS AND SPACE ADMINISTRATION
WASHINGTON, D. C. 20546

OFFICIAL BUSINESS

FIRST CLASS MAIL

POSTAGE AND FEES PAID
NATIONAL AERONAUTICS AND
SPACE ADMINISTRATION

POSTMASTER: If Undeliverable (Section 158 Postal Manual) Do Not Return

"The aeronautical and space activities of the United States shall be conducted so as to contribute . . . to the expansion of human knowledge of phenomena in the atmosphere and space. The Administration shall provide for the widest practicable and appropriate dissemination of information concerning its activities and the results thereof."

—NATIONAL AERONAUTICS AND SPACE ACT OF 1958

NASA SCIENTIFIC AND TECHNICAL PUBLICATIONS

TECHNICAL REPORTS: Scientific and technical information considered important, complete, and a lasting contribution to existing knowledge.

TECHNICAL NOTES: Information less broad in scope but nevertheless of importance as a contribution to existing knowledge.

TECHNICAL MEMORANDUMS: Information receiving limited distribution because of preliminary data, security classification, or other reasons.

CONTRACTOR REPORTS: Scientific and technical information generated under a NASA contract or grant and considered an important contribution to existing knowledge.

TECHNICAL TRANSLATIONS: Information published in a foreign language considered to merit NASA distribution in English.

SPECIAL PUBLICATIONS: Information derived from or of value to NASA activities. Publications include conference proceedings, monographs, data compilations, handbooks, sourcebooks, and special bibliographies.

TECHNOLOGY UTILIZATION PUBLICATIONS: Information on technology used by NASA that may be of particular interest in commercial and other non-aerospace applications. Publications include Tech Briefs, Technology Utilization Reports and Notes, and Technology Surveys.

Details on the availability of these publications may be obtained from:

SCIENTIFIC AND TECHNICAL INFORMATION DIVISION

NATIONAL AERONAUTICS AND SPACE ADMINISTRATION

Washington, D.C. 20546